Dynamical Evolution of Intense Ierapetra Eddies on a 22 Year Long Period

Artemis Ioannou, Alexandre Stegner, Briac Le Vu, Isabelle Taupier-Letage, Sabrina Speich

AGU PUBLICATIONS

JGR

Journal of Geophysical Research: Oceans

RESEARCH ARTICLE

10.1002/2017JC013158

Key Points:
- Dynamical characterization of Ierapetra eddies
- Seasonal and interannual eddy variability
- Cyclogeostrophic balance

Correspondence to:
A. Ioannou,
artemis.ioannou@lmd.polytechnique.fr

Citation:
Ioannou, A., Stegner, A., Le Vu, B., Taupier-Letage, I., & Speich, S. (2017). Dynamical evolution of intense Ierapetra eddies on a 22 year long period. *Journal of Geophysical Research: Oceans*, *122*, 9276–9298. https://doi.org/10.1002/2017JC013158

Received 6 JUN 2017
Accepted 29 OCT 2017
Accepted article online 2 NOV 2017
Published online 30 NOV 2017

Dynamical Evolution of Intense Ierapetra Eddies on a 22 Year Long Period

Artemis Ioannou[1], Alexandre Stegner[1], Briac Le Vu[1], Isabelle Taupier-Letage[2], and Sabrina Speich[3]

[1]Laboratoire de Météorologie Dynamique, CNRS Ecole Polytechnique, Palaiseau, France, [2]Aix Marseille Université, CNRS/INSU, Université de Toulon, IRD, Mediterranean Institute of Oceanography (MIO) UM, La Seyne, France, [3]Laboratoire de Météorologie Dynamique, CNRS Ecole Normale Supérieure, Paris, France

Abstract Considered as wind forced, the recurrent formation of Ierapetra eddy affects the Eastern Mediterranean Sea circulation. Even though this large, coherent, and long-lived anticyclone has been extensively studied, there are only few quantitative information on its dynamical characteristics. The main goal of this study is to quantify the Ierapetra eddies (IEs) intensity and examine their seasonal and interannual variability over a 22 year period (1993–2014). We choose the automatic eddy detection algorithm AMEDA to estimate the main IEs dynamical parameters such as their size, their intensities, and their lifetimes. Applied to daily AVISO altimetric products, the AMEDA allows a full eddy characterization providing additional information on vortex velocity profiles as well as on merging and splitting events. Among the years of observations, the IEs Rossby number experience a strong variability and could vary by a factor 4 ($Ro = 0.07–0.27$). This is mainly due to the eddy velocity variations rather than size variations. Moreover, we found that after their formation IEs could reintensify. This intensification process may lead to a doubling of the vortex intensity in less than 4 months. That extra input of energy coincides with the Etesian winds period. Such high intensities are not expected from large-scale anticyclones and require cyclogeostrophic corrections. Considering this ageostrophic part, the maximum values of the core vorticity were derived and we found that the IEs might sometimes exhibit a negative potential vorticity core. Evidences on the eddy intensity from two oceanographic campaigns suggest that the IEs are probably more intense than we even estimate.

1. Introduction

The regional circulation in the Eastern Mediterranean Sea (EMS) is a complex system dominated by large gyres and long-lived eddies. The investigation of the EMS started with the pioneering work of Nielsen (1912) a hundred years ago. Nielsen (1912), Ovchinnikov (1966), Ovchinnikov et al. (1976), and Lacombe and Tchernia (1972) depicted an overall counterclockwise circulation in the whole basin. Since then, several oceanographic campaigns and in situ measurements were conducted with higher spatial sampling that revealed the existence of mesoscale features especially large-scale anticyclones. The POEM (Physical Oceanography of the Eastern Mediterranean) project used a large hydrographic data base collected during 1985–1987 (Malanotte-Rizzoli et al., 1997; Robinson et al., 1987, 1991, 1992; Robinson & Golnaraghi, 1993; Schroeder et al., 2012) to derive the geostrophic surface circulation and identify several gyres and mesoscale eddies considered as quasi-permanent or recurrent. Indeed, the temporal sampling of these hydrographic surveys could not capture the dynamical evolution of the mesoscale eddies. However, the technological development of remote sensing measurements had opened a new window for the detection of surface eddies from 1980s. The satellite sea surface temperature (SST) images first (Matteoda & Glenn, 1996; Millot, 1985; Puillat et al., 2002; Taupier-Letage et al., 2003; Zervakis et al., 2003) and later the sea surface height (SSH) maps (Amitai et al., 2010; Isern-Fontanet et al., 2006; Mkhinini et al., 2014; Pascual et al., 2007; Rio et al., 2007) provide an efficient way to identify the long-lived eddies and follow their trajectories. The analysis of Lagrangian drifters were also used to quantify the intensity of the surface eddies, for instance the typical angular velocities within the eddy core (Gerin et al., 2009; Matteoda & Glenn, 1996; Menna et al., 2012; Mkhinini et al., 2014; Sutyrin et al., 2009). However, the drifters data or the various in situ measurements available, CTD transects or vessel mounted ADCP sections, are still sparse especially in the Eastern Basin. It is only recently that the combination of the high-resolution altimetric maps (gridded at 1/8° in the Mediterranean Sea) with automatic eddy detection and

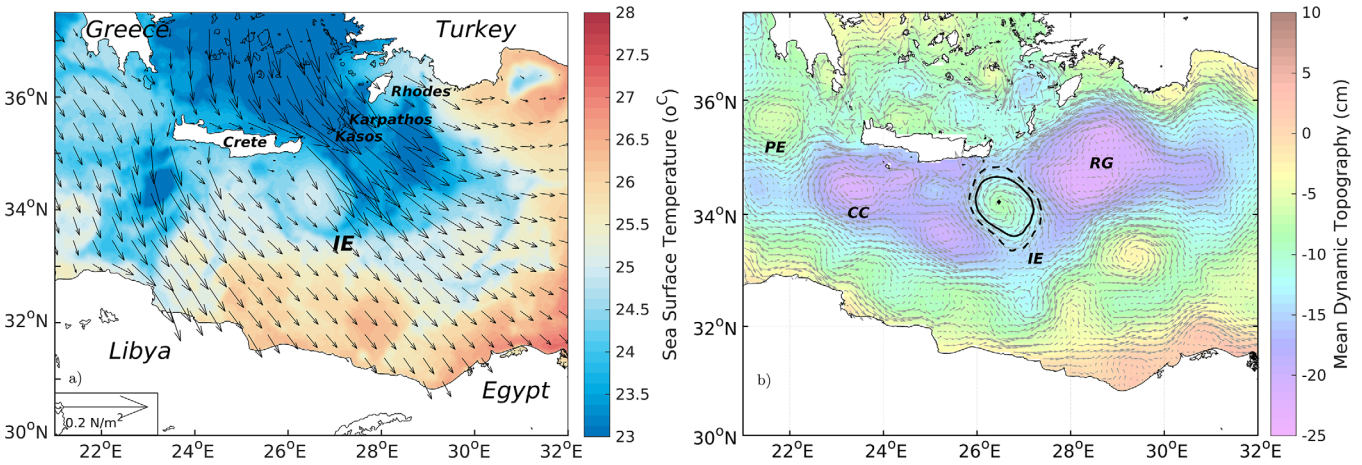

Figure 1. (a) Sea surface temperature in the Eastern Mediterranean Sea the 4 October 2006 (JPL MUR MEaSUREs Project, 2010). The warm core of the Ierapetra eddy (IE) is centered at (26.5°E, 34.2°N) while the predominant direction of the Etesian winds between Crete and Kasos Island is indicated with the black arrows. The vectors represent climatological (1993–2012) wind stress components of the summer months (Tramblay et al., 2013). (b) Location of the climatological mean Ierapetra eddy (IE), the Pelops eddy (PE), the Cretan Cyclone (CC), and the Rhodes Gyre (RG) on the 20 years (1993–2015) mean dynamic topography (MDT) of the Eastern Mediterranean Sea. The characteristic contour of the IE is plotted with a black solid line while the black dashed line indicates the last closed contour.

tracking algorithms allow to quantify more adequately the dynamical evolution and the temporal variability of mesoscale eddies over long time periods.

Among the various eddies detected in the EMS, the Ierapetra anticyclone is probably one of the most fascinating structures. It has one of the strongest signal on the SSH (Amitai et al., 2010; Isern-Fontanet et al., 2006; Mkhinini et al., 2014; Rio et al., 2007) and quite often an amazing signature on the SST. Figure 1a is a typical example of the strong SST pattern induced by this anticyclone. This intense and large-scale anticyclone is generally formed during the summer months at the south-east corner of Crete. The Ierapetra eddy (IE) was first identified from the POEM hydrographic data by Theocharis et al. (1993), then, by Horton et al. (1994) based on two extensive airborne expendable bathythermograph (AXBT) surveys conducted during December 1991 and July 1992. Horton et al. (1994) and Fusco et al. (2003) suggested that this intense anticyclone is a consequence of the strong Etesian winds being blocked by the Cretan orography. The seasonal correlation, averaged over 20 years, between the formation area of the IE and the localized area of negative wind stress curl seems to confirm this hypothesis Mkhinini et al. (2014).

Matteoda and Glenn (1996) were the first to perform a quantitative analysis of several years of satellite imagery and a detailed examination of four drifting buoys to monitor five recurrent mesoscale eddies in the EMS. They found that the IE, which was observed in 85% of the AVHRR images during the 4 years period (1990–1994), was the most persistent of them. The frontal boundaries on the SST fields were digitized to perform a statistical analysis of the typical eddy size, i.e., the mean radius of the quasi-circular patch of warm water. The statistical distribution of this radius for the Ierapetra anticyclone range between 25 and 65 km with a mean value of 48 km which is much larger than the local deformation radius (R_d = 10–12 km) while its center location clusters around (34.3°N, 26.7°E). The looping buoy trajectories of one surface drifter trapped inside the IE for 2 months were analyzed. The mean orbital period of the clockwise elliptical loops was about 3 days and associated with a mean negative surface vorticity around $\zeta = -5 \times 10^{-5}\ s^{-1}$. This first estimation of the core vorticity of IE is quite large in comparison with the local Coriolis parameter f and corresponds to a relative vorticity of $\zeta/f = -0.8$. Matteoda and Glenn (1996) also observed the signature of inertial waves inside two mesoscale anticyclones. Surprisingly, no other data analysis or in situ campaign tried to confirm such strong (negative) vorticity value which indicates a cyclogeostrophic balance for the large Ierapetra anticyclone. A more recent study Mkhinini et al. (2014) approximates the IE with a gaussian profile and shows that its intensity may vary significantly during the year. The typical speed radius of the eddy range from 35 to 50 km while weaker values were found for the relative core vorticity ($-0.45 \leq \zeta/f \leq -0.25$) and the Rossby number (Ro = 0.08–0.15). Hence, the real intensity of the IE and how it varies during the eddy lifetime are still open questions.

The use of altimetric data, which are not affected by cloud coverage as the SST images, provides one of the most powerful time series to analyse the seasonal variability of mesoscale structures. The pioneering study

of Larnicol et al. (1995) uses the TOPEX/POSEIDON (T/P) altimetric data to study the mean sea level variations. Using suboptimal space-time objective analysis, the seasonal variability of the sea level anomaly (SLA) of the Mediterranean Sea was quantified. Moreover, strong anticyclonic mesoscale signals, such as the Alboran gyres or the Ierapetra eddy, were shown to have a clear seasonal variability, with a maximum in summer. However, the SLA is an indirect measure of the eddy intensity and high-resolution maps were needed to estimate correctly the geostrophic surface velocities which are proportional to the gradients of the sea surface height (SSH). Few years later, the combined altimetric tracks of T/P and ERS-1/2 provide higher resolution maps of the SLA (Larnicol et al., 2002). This study confirms that the IE constitutes the most intense signal of the EMS variability with a maximum intensity in August. Besides, this study mentions a possible merging of the IE with another anticyclone in 1995.

The thorough analysis of SST images during the period 1985–2001 performed by Hamad et al. (2005, 2006) shows that IE can be tracked for years, sometimes several hundreds of km away from the main formation area and interact with the general circulation (Hamad et al., 2005, 2006; Puillat et al., 2002). Besides, they observed that IEs can merge with the IE of the forthcoming year coexist or merge with another eddy, with life durations above 3 years. These studies emphasize the complex flow circulation in the Levantine basin driven by the turbulent eddy field. The large mesoscale patterns and especially the IE cannot be seen as quasi-permanent and steady features that stay at their formation area. However, such analysis based on the temperature signature of the mesoscale eddies at the sea surface cannot provide quantitative information for their intensity.

The improvements on eddy detection and tracking algorithms (Chaigneau et al., 2009; Chelton et al., 2011; Le Vu et al., 2017; Mkhinini et al., 2014; Nencioli et al., 2010) allow to characterize the main dynamical parameters of the detected eddies such as their size, their maximal azimuthal velocities and therefore their typical Rossby numbers. Moreover, the most recent algorithms provide new methods to identify the specific splitting and merging events (Du et al., 2014; Le Vu et al., 2017; Li et al., 2014). The recent study of Mkhinini et al. (2014) used a hybrid eddy tracking algorithm applied on the surface geostrophic velocity gridded at 1/8° for the Mediterranean Sea (AVISO products) to follow the dynamical variations and the trajectories of long-lived mesoscale eddies in the Eastern Basin. The generation area of the IE anticyclones for the 1994–2014 period was clearly identified in the south-east of Crete during summer months when the mean wind stress curl, averaged over 20 years, reaches the strongest negative values. Besides, it was shown that the intensity of the IE could vary by at least a factor 2 between July and October 2006. This example shows that the Rossby number of this specific anticyclone may experience a strong seasonal variability.

According to the previous studies, there are a few evidences that the IE experience significant variations of its intensity. Besides, such large mesoscale anticyclones ($R \simeq 2$–$3R_d$) are generally assumed to satisfy the geostrophic balance while for the IE it seems that the relative core vorticity could reach strong negative values. Surprisingly, very few studies quantify accurately the intensity and the dynamical evolution of this very robust and coherent anticyclone which can strongly impact the surface circulation of the EMS. There are still many open questions and we do not know precisely if an IE is formed every year? How long it could survive? How far it could travel in the Eastern Basin? Or what could be its maximal intensity? Therefore, the main goal of this study is to estimate by the combination of the most recent altimetric products and in situ measurements the surface velocity structure and the dynamical variability of the Ierapetra eddies. The paper is organized as follows. In section 2, we describe the various data sets and the specifications of the eddy detection and tracking algorithm AMEDA that we used. Section 3 presents a throughout analysis of the vortex intensity deduced from AVISO products and its seasonal and/or interannual variability over the 1993–2015 period. The lifetimes, typical trajectories, and specific events are detailed in section 4. Next, several comparisons with available in situ measurements are carried out in section 5. Finally, we sum up, in section 6, the main dynamical characteristics of the IE and conclude on their potential impacts on the local transport and mixing.

2. Data and Methods

2.1. Eddy Detection

2.1.1. Remote Sensing With Sea Surface Height

To quantify the temporal evolution of the Ierapetra eddies, we used the geostrophic velocity fields, produced by Ssalto/Duacs and distributed by AVISO and derived from the Absolute Dynamical Topography (ADT). Unlike the Seal Level Anomaly (SLA), which represents the variable part of sea surface height, the

ADT is the sum of this variable part and of the constant part averaged over a 20 year reference period. The all-sat-merged series distributed for the Mediterranean Sea combines, for the years 1993–2015, up-to-date data sets with up to four satellites at a given time, using all missions available (Topex/Poseidon, ERS-1 and −2, Jason-1 and −2, Saral, Cryosat-2, and Envisat missions). This merged satellite product, for the Mediterranean Sea, is projected on a 1/8° Mercator grid, with a time interval of 24 h.

We should note that the horizontal resolution of the 1/8° gridded velocity fields ($dX \simeq 12$ km) cannot fully resolve the internal deformation radius R_d which is around 10–15 km in the Eastern Mediterranean Sea (Escudier et al., 2016). However, the surface signature of large mesoscale eddies with a typical radius that exceed the deformation radius are generally detected (Amitai et al., 2010; Isern-Fontanet et al., 2006; Mkhinini et al., 2014; Pascual et al., 2007; Rio et al., 2007). But, we should keep in mind that the spatiotemporal heterogeneity of the altimetric tracks of satellites, could also induce spurious eddy detection or systematic bias to the eddies intensity.

2.1.2. AMEDA Eddy Detection Algorithm

We use in this study the Angular Momentum Eddy Detection and tracking Algorithm (AMEDA) which is based on physical parameters and the geometrical properties of the velocity field (Le Vu et al., 2017). We apply this algorithm to the surface geostrophic velocities provided by AVISO (Figure 2a) to identify the eddy centers and quantify their intensity. The eddy centers correspond to an extremum of the local normalized angular momentum. The streamlines surrounding this center are then computed (Figure 2b). The mean radius $\langle R \rangle$ and the mean velocity $\langle V \rangle$ are evaluated for each closed contour. As described by equation (1), the mean radius $\langle R \rangle$ is defined as the equivalent radius of a circular disc with the same area A as the one delimited by the closed streamline, while the mean velocity amplitude $\langle V \rangle$ is derived from the circulation along the closed streamline C, where L_p is the streamline perimeter, equation (2).

$$\langle R \rangle = \sqrt{\left(\frac{A}{\pi}\right)} \tag{1}$$

$$\langle V \rangle = \frac{1}{Lp} \oint_C V dl \tag{2}$$

We plot in Figure 2c the pair of mean eddy velocity $\langle V \rangle$ and mean radius $\langle R \rangle$ for each closed contour. We can see on this example that the mean velocity increases when the radius increases until a maximum velocity V_{max} is reached. The corresponding radius is named R_{max}, also called the *speed radius* in previous studies (Chelton et al., 2011). The *characteristic contour* of the detected eddy (blue contours in Figure 2) is

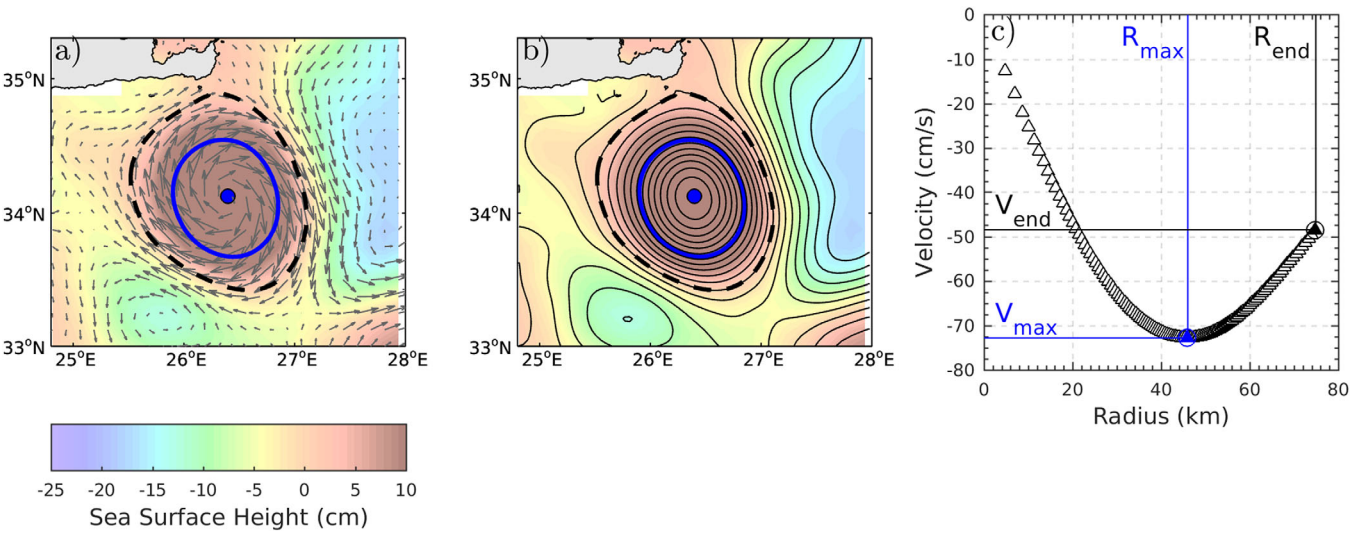

Figure 2. (a) The characteristic contour (solid blue line) and the last contour (black dashed line) calculated by the AMEDA for an Ierapetra eddy. The background colors correspond to the ADT map while the black vectors to the surface geostrophic velocities. (b) The streamlines associated with the velocity field and the correspondence with the characteristic (solid blue line) and the last closed contour (black dashed line). The velocity profile $\langle V \rangle = F(\langle R \rangle)$ deduced from the streamlines analysis is plotted in (c). We use here negative values for the mean velocities $\langle V \rangle$ of anticyclones.

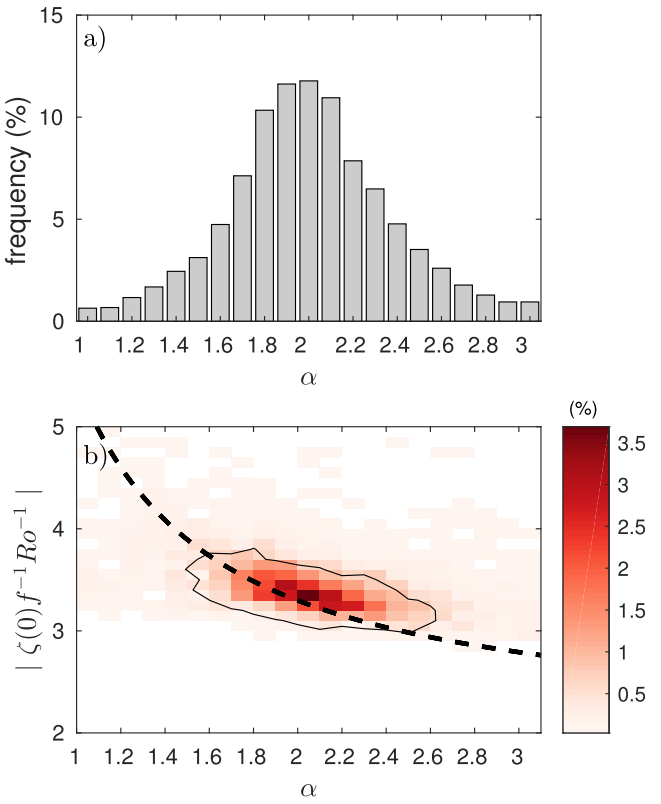

Figure 3. (a) Distribution of steepness parameter α for Ierapetra eddies when the ellipticity is lower than $\varepsilon < 0.3$. The impact of the steepness parameter α on the dimensionless ratio $\zeta(0)f^{-1}Ro^{-1}$ is plotted in (b). The black dashed line corresponds to equation (5) while the colors illustrate the density distribution of the dynamical values obtained with the AMEDA for the Ierapetra eddies. The black contour delimits ~70% of the data.

associated with the closed streamline of maximal speed. After this maxima, the azimuthal speed of the eddy decreases until the last closed contour (black dashed contour in Figure 2) is reached. When V_{max} and V_{end} are too close from each other ($V_{end} > 0.97V_{\max}$) the *characteristic contour* is then plotted with a dashed line to indicate that the maximal velocity is reached at the edge of the eddy.

We mainly use in this study R_{max}, V_{max}, and the velocity profile $\langle V \rangle = F(\langle R \rangle)$ to quantify respectively the size, the intensity and the horizontal shape of the eddy. We should note that V_{max} is positive for cyclones and negative for anticyclones. The eddy intensity is estimated with the use of the absolute value of the vortex Rossby number as follows:

$$Ro = \left| \frac{V_{\max}}{R_{\max} f} \right| \tag{3}$$

Moreover, the velocity profiles are fitted with a generic function:

$$V_\theta(r) = \frac{V_{\max}}{R_{\max}} r\, e^{(1-(r/R_{\max})^\alpha)/\alpha} \tag{4}$$

where $r = \langle R \rangle$ and α is the steepness parameter. Such generic profiles were used by Carton et al. (1989) and Stegner and Dritschel (2000) to study the stability of isolated eddies. Note that when $\alpha = 2$ the velocity profile corresponds to a Gaussian vortex. We found that the generic velocity profile equation (4) provides a high correlation fit above 98% ($R^2 \geq 0.98$) for 88% of the IE eddies when the steepness parameter alpha is correctly adjusted. Figure 3a shows the distribution of the adjusted steepness parameter ranging from $\alpha = 1$–3 with a mean value $\alpha = 2$ and a standard deviation σ of 0.43. Once we quantify the Rossby number and the steepness parameter, we can estimate for circular eddies based on equation (4) the relative core vorticity $\zeta(0)/f$ according to the relation:

$$\frac{\zeta(0)}{f} = \frac{1}{f}\left(\frac{\partial V_\theta}{\partial r} + \frac{V_\theta}{r}\right)_{r=0} = 2e^{1/\alpha} Ro \tag{5}$$

We could then expect that the ratio of the core vorticity divided by the vortex Rossby number $\zeta(0)f^{-1}Ro^{-1}$ depends only on the velocity profile, in other words the α parameter. Figure 3b confirms that equation (5) is in correct agreement with the dynamical values obtained by the AMEDA from the AVISO data sets. We also interpolate the characteristic contour by an ellipse and estimate an equivalent ellipticity $\varepsilon = 1 - b/a$ (also called the flattening parameter) where b is the semi minor axis and a is the semi major axis. Moreover, the tracking procedure of the AMEDA identifies merging and splitting events (for more details see Le Vu et al., 2017). Hence, we are able to track the long-term evolution of mesoscale eddies even if they merge or split during their lifetime.

2.1.3. Thermal Satellite Images

Although impaired by the cloud cover, satellite images from NOAA/AVHRR have been used for the 1980s to spot and track eddies, and contributed to general circulation studies. The use of thermal images (hereafter SST: sea surface temperature) for circulation studies and their limitations are detailed in Taupier-Letage (2008). For this study only a few cases of IEs have been tracked with SST images, sometimes on limited periods, in order to check both methods results.

2.2. In Situ Observations/Oceanographic Campaigns

2.2.1. EGYPT Campaign

The EGYPT-1 campaign was held in April 2006 within the frame of the EGYPT (Eddies and GYres Paths Tracking) and EGITTO observational programs to study the role of the mesoscale eddies on the general circulation in the Eastern Basin (Taupier-Letage et al., 2007). Among the 125 CTD casts performed, one section crossed the Ierapetra eddy generated in 2005 (Taupier-Letage, 2008), with 18 CTD profiles every 8–10 km

along a total distance of 180 km. This hydrologic transect provides useful information on the vertical structure of IE05 and allows to compute the geostrophic velocities across the anticyclone. Furthermore over the 90 surface drifters (with 15 m sockets) launched in the EGYPT/EGITTO program (Gerin et al., 2009), 5 were deployed in IE05, 2 of which remained trapped inside the anticyclone for almost 3 months.

2.2.2. BOUM Campaign

The BOUM (Biogeochemistry from the Oligotrophic to the Ultraoligotrophic Mediterranean) campaign (http://mio.pytheas.univamu.fr/BOUM/) was held in summer 2008, from the 16 June to the 20 July, with the French Research Vessel l'Atalante. The cruise consisted of a 3,000 km transect from the Rhone River mouth (Western Mediterranean) to the Eratosthenes Seamount (eastern Mediterranean). This eastward-westward BOUM transect, covering essentially the southern part of the basins, enabled the physical and biogeochemical states of the EMS to be observed during the summer 2008 (Moutin & Prieur, 2012). Among the 30 stations that were performed along this transect, we focus on the few ones around the IE05 that was crossed in June 2008. One CTD and LADCP cast was performed inside the eddy core the 23 June. Moreover, Vessel-Mounted Acoustic Doopler Curent Profilers (VMADCP) were used to obtain vertical profiles of current speed and direction in the upper layer. We focus on the VMADCP data when the ship crossed IE05's core the 30 June on its way back to the Western Mediterranean. The maximum depth of VMADCP measurements was about 200 m.

3. Dynamical Evolution of Ierapetra Anticyclones

3.1. Climatological Signature of IEs

The 20 year averaged mean dynamic topography (MDT) of the Eastern Mediterranean Sea is plotted in Figure 1b. It exhibits the recurrent and energetic patterns of the North Levantine region: the IE centered at (27°E, 34.3°N), the Rhodes Gyre (RG) centered at (28°E, 34.5°N), the Cretan Cyclone (CC) centered at (25°E, 34°N), and the Pelops eddy (PE) centered at (21.5°E, 35.8°N). The IE is marked with two black contours: the characteristic (solid line) and the latest contour (dashed line), respectively. It has, according to the MDT, a mean diameter of $\bar{R}=55$ km and relatively weak intensity of $\overline{Ro}=0.02$. However, many studies have shown that the IE is not stationary (Hamad et al., 2005, 2006; Larnicol et al., 1995, 2002). It experiences seasonal variations and could move over long distance away from its generation point. Hence, since we know that the IE moves around its formation area or escapes far away, this 20 years average of the surface circulation will strongly underestimate its intensity.

The density of the center positions of the IEs, during the 20 year period (1993–2012), is shown in Figure 8d. More than 56% of the IE centers are located inside the last contour (black dashed line). Therefore, we named this area: the *IE area*. This statistical distribution shows that the IEs could stay a long time in the same area and strongly impact the regional circulation south of Crete. The analysis of the first Empirical Orthogonal Function (EOF) of the SLA fields performed by Amitai et al. (2010) confirms that the principal feature of the EMS is the strong Ierapetra anticyclone. However, to estimate precisely the intensity and the dynamical evolution of this large-scale anticyclone, we need to process the daily products provided by AVISO.

3.2. Seasonal Variability

In order to investigate the seasonal variability of mesoscale eddies, we compute the monthly means of the main dynamical parameters such as the dimensionless radius R_{max}/R_d ($R_d=10$ km), the Rossby number Ro or the ellipticity ε. We chose the Ierapetra eddy formed in 1998 (IE98) to illustrate the seasonal evolution of these dynamical parameters in Figure 4. This anticyclone was initially detected in the AVISO products the 17 July 1998 and its surface signature was tracked by the AMEDA during more than 2 years till October 2000. The eddy center stays in the *IE area* for 23 months and moves inside it with a drifting velocity that does not exceed 1.2 km d^{-1}. Then, during the last 5 months of detection the IE98 drifted south toward the Egyptian slope with a mean speed of $\sim$2.5 km d^{-1}.

Figure 4 reveals various stages in the dynamical evolution of the IE98. The first stage corresponds to the eddy formation which occurs in summer 1998. We should note that, if a smaller structure exists before that period it may not have a signature on the altimetric products. However, with no evidence of such preexisting structure, we will consider that the first detection obtained with the eddy detection algorithm corresponds to the formation point of the IE. This is coherent with the SST analysis which shows that IE98 is

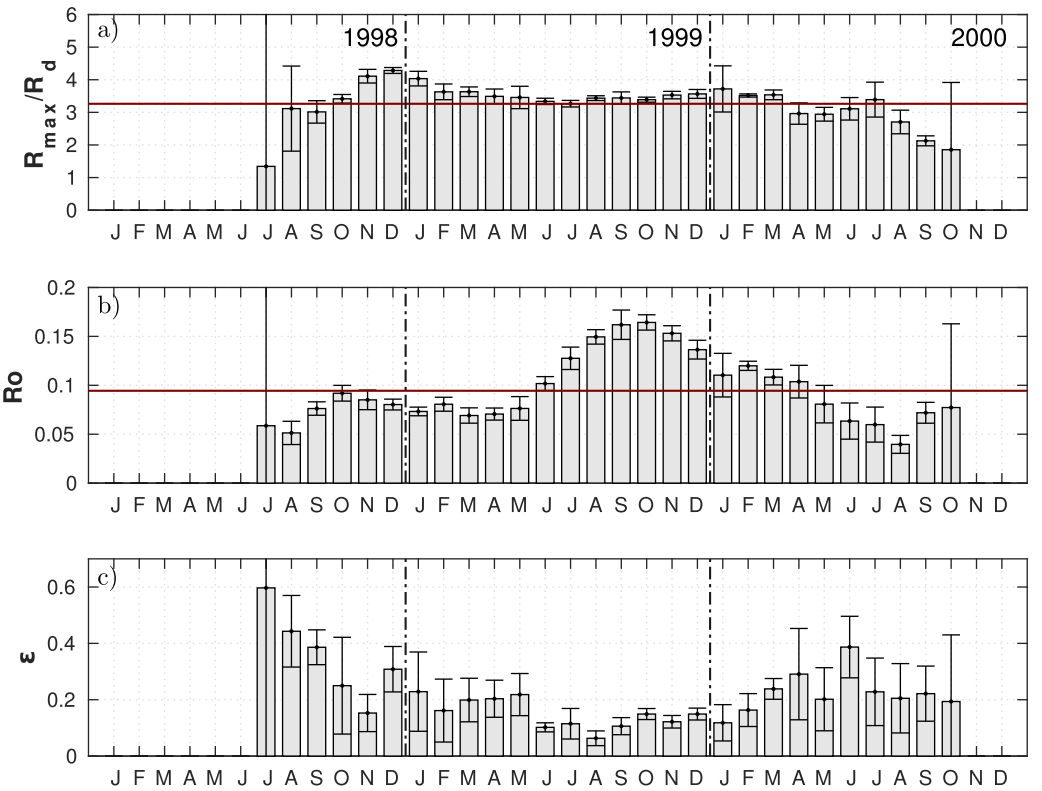

Figure 4. Temporal evolution of (a) the relative size (R_{max}/R_d), (b) the Rossby number (Ro), and (c) the ellipticity ($\varepsilon = 1 - a/b$)of the Ierapetra anticyclone formed in 1998 (IE98). The error bars correspond to the monthly RMS of the parameters while the horizontal lines indicate the mean values for the eddy lifetime.

created after the 5 July and before the 17 August 1998 (Hamad et al., 2006, Figures 12 and 13). During this initial period, from July to October 1998, both the radius and the intensity of the anticyclone increase while the ellipticity of the structure, which is initially high, decays (Figure 4c). As we can see in Figure 5a, the characteristic contour of the IE98 is indeed strongly elliptical during this formation stage. In October–November, the IE98 reaches a "mature stage," where both the size and the Rossby number reach a plateau. The IE98 is then fully developed with an intensity of $Ro = 0.1$ and a radius $R_{\max} = 37$ km which is 3.5 times larger than the local deformation radius ($R_d = 10$ km). For simplicity, this stage will be refereed as *maturity stage*. A snapshot of the eddy structure which reaches its maturity in October is shown in Figure 5b. At this stage, the characteristic contour is quasi-circular and both the location and the size are in correct agreement with the SST signature (Hamad et al., 2006). Then the IE98 survives the following year (1999), keeping roughly the same size and intensity. This period corresponds to a quasi-steady stage, and according to Figures 4 and 5, we do not see strong changes from October 1998 to May 1999. During the following summer, IE98 is thus still located SE of Crete and prevents the creation of a new Ierapetra anticyclone in 1999.

Then, in less than 4 months, from June to September 1999, the intensity of the IE98 doubles while its characteristic radius R_{max} stays constant. Such intensification of a preexisting Ierapetra anticyclone, with a monthly mean Rossby number that rises from $Ro = 0.08$ in May up to $Ro = 0.16$ in September 1999 was never studied or emphasized before. The fact that the geometrical characteristics of the eddy, especially its radius and its ellipticity, remain unchanged may explain why such event, that has no signature on the SST or the chlorophyll patterns, can hardly be detected by satellite imagery. The analysis of altimetric products is therefore the only way to detect such variations in the intensity. Amitai et al. (2010) exhibits a strong EKE associated with the Ierapetra anticyclone in fall 1999 but did not make the link with the IE98 formed the preceding year. More recently, Mkhinini et al. (2014) mentioned the intensification of a preexisting IE in summer 2006 but did not study the phenomena in details. These specific events will be refereed to what follows as *intensification* stages. Our analysis shows that such *intensification* occurs at least four times during the 22 years period: in 1995 (for IE94), 1999 (for IE98), 2001 (for IE00), and 2006 (for IE05). This specific event

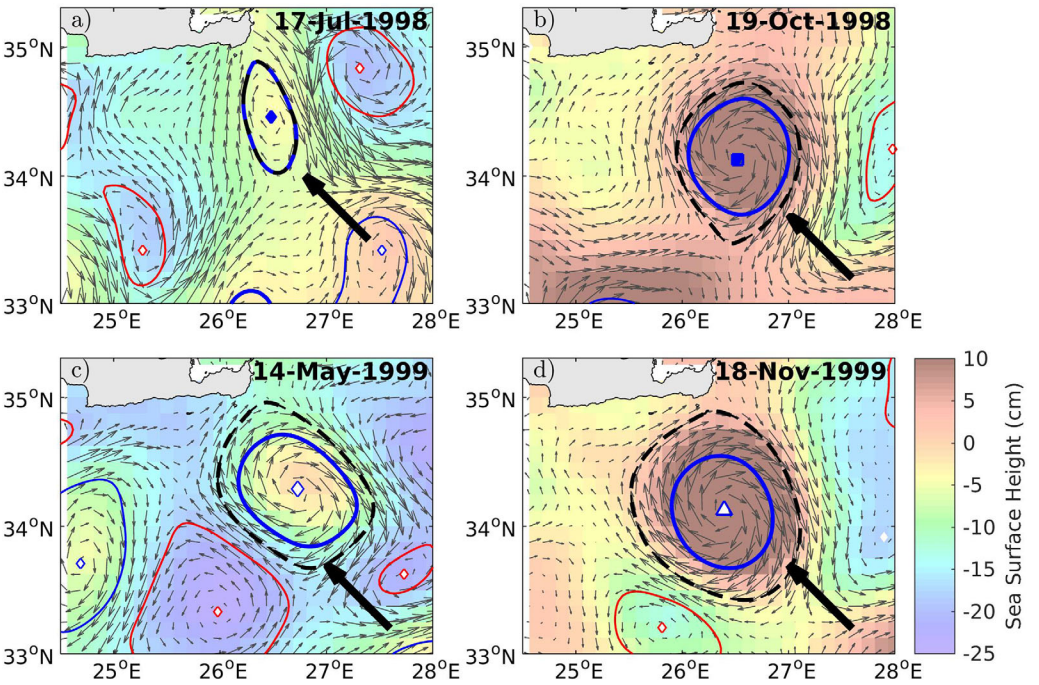

Figure 5. Snapshots of the temporal evolution of the IE98. The formation of the eddy (a) occurs in July 1998, (b) it reaches maturity in October 1998 and (c) after a quasi-steady stage the intensity of the anticyclone increases strongly from June 1999 and (d) reaches its maximum intensification in September 1999. The background colors correspond to the ADT while the gray arrows correspond to the surface geostrophic velocities. The characteristics contours computed by the AMEDA are plotted in red and blue for cyclonic and anticyclonic eddies, respectively.

always occurs the next year after the IE reached its *maturity* stage. We should note that the increase of the vortex intensity coincide with the period of strong Ethesian winds, while the maximum of *intensification* occurs in September–October. This coincidence is striking, but it cannot ensure that this additional input of energy, inside a preexisting IE, is only due to the wind forcing. After this *intensification* a decay in the Rossby number is usually observed. As it is shown in Figure 4b, it takes 8 months for the IE98 to reduce its intensity by a factor 2. The decay could be even shorter, as in 1995 and 2000 when it took less than 4 months for an equivalent reduction of the Rossby number.

3.3. Cyclogeostrophic Balance of IE

Our first analysis reveals that the Ierapetra anticyclones often reach Rossby numbers that exceed $Ro = 0.15$ during the *maturity* or the *intensification* stages. Such Rossby numbers seem small but they are not negligible and we could wonder if the geostrophic balance, which is a major assumption for the derivation of surface velocity from altimetric data sets, still holds. The study of Penven et al. (2014) has shown that the effects of centrifugal acceleration are significant when deriving velocities from AVISO gridded altimetry in the Mozambique Channel. Moreover, the analysis of Tuel et al. (2016) has shown that for moderate values of the Rossby number the centrifugal correction might be significant especially for circular anticyclones. For instance, a Rossby number around $Ro \simeq 0.15$ could lead to a systematic underestimation of the azimuthal velocities (–35%) for a Gaussian anticyclone (i.e., $\alpha = 2$).

We have noticed, for the IE, that the highest value of the Rossby numbers generally coincides with smallest ellipticity values (as shown in Figure 4). Hence, it makes sense to consider quasi-circular Ierapetra anticyclones with small ellipticity $\varepsilon < 0.1$. At the first order of approximation we will then assume a steady circular structure that satisfies the cyclogeostrophic balance:

$$\frac{V_\theta^2}{r} + fV_\theta = g\partial_r\eta = fV_g \tag{6}$$

where $V_\theta(r)$ is the azimuthal velocity, $\eta(r)$ is the sea surface deviation, and $V_g(r)$ the geostrophic velocity corresponding to the standard AVISO products. Note that for an anticyclone (cyclone), the azimuthal

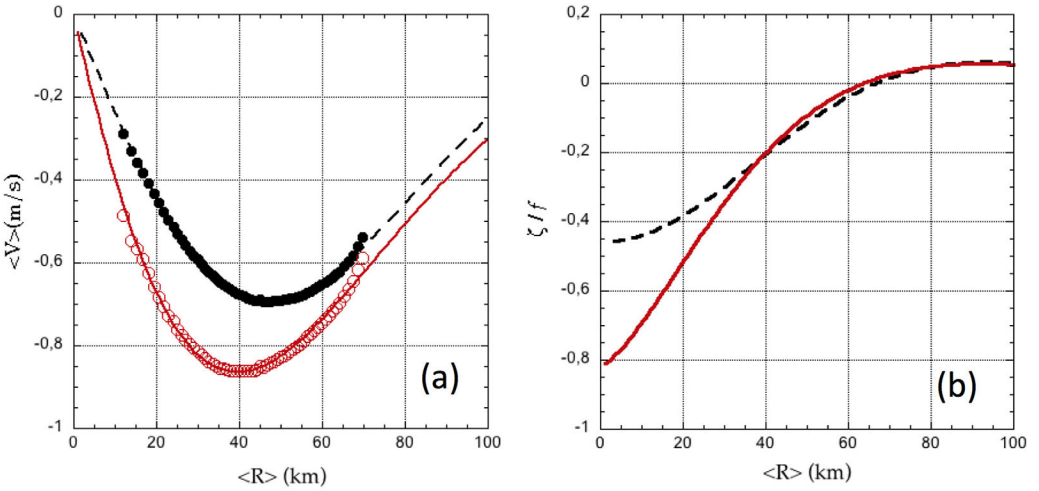

Figure 6. (a) Velocity and (b) vorticity profiles of the IE98 the first of September 1999 when the ellipticity is weak $\varepsilon=0.06$. The geostrophic profile is depicted with the black dotted line while cyclogeostrophic profile, calculated with equation (6), is shown in red. The Rossby number associated with the cyclogeostrophic profile $Ro = 0.21$ is higher than the geostrophic one $Ro = 0.15$.

velocities are negative (positive). It is then quite simple to calculate the cyclogeostrophic velocity V_θ from a circular geostrophic velocity profile $V_g=\langle V\rangle=F(\langle R\rangle)$, where $\langle V\rangle$ is the mean velocity averaged along each closed streamline of mean radius $\langle R\rangle$ (see Figure 2c). Solving the second order equation (6) we get

$$\langle V_\theta\rangle=-\frac{f\langle R\rangle}{2}\left(1-\sqrt{1+\frac{4V_g}{f\langle R\rangle}}\right) \tag{7}$$

Figure 6a shows the impact of the centrifugal correction on the velocity profile for the IE98 in early September 1999 when the vortex is quasi-circular ($\varepsilon=0.06$) and the Rossby number reaches $Ro = 0.15$. The black filled circles correspond to the mean values $(\langle R\rangle, \langle V\rangle)$ computed from the geostrophic streamlines while the red ones are obtained from the cyclogeostrophic equation (7). The maximal velocity V_{max} increases by 25% when the centrifugal correction is added while the speed radius R_{max} is reduced by 10% and therefore the vortex Rossby number rises up to $Ro = 0.21$. Both velocity profiles are then fitted with the generic function equation (4). The shape of the geostrophic profile is close to a Gaussian vortex with a steepness parameter $\alpha=2.2$. We then use the equation:

$$\zeta(r)=\partial_r\langle V_\theta\rangle+\frac{\langle V_\theta\rangle}{r} \tag{8}$$

to estimate the vorticity profiles of the circular eddies (Figure 6b). The amplitude of the centrifugal correction is even more pronounced for the vorticity than the velocity. Indeed, the relative core value of the geostrophic profile is around $\zeta(0)/f=-0.45$ while the cyclogeostrophic solution goes down to $\zeta(0)/f=-0.8$. Even if the pioneering analysis of Matteoda and Glenn (1996) indicates such large vorticity values it is still quite unexpected that a large mesoscale anticyclone ($R_{\max}\simeq 4R_d$) could reach such negative vorticity values in his core. Our analysis confirms that during the *maturity* or *intensification* stages the IE are not geostrophic and therefore the cyclogeostrophic balance should be taken into account to estimate correctly their intensity.

3.4. Interannual Variability

3.4.1. Variability in the IE's Intensity

In order to study the interannual variability of the IEs, we consider the maximum intensity reached by the anticyclones during their lifetime. For the 22 years of analysis, 16 IEs were identified and the maximum values of the Rossby number measured at the *maturity* or the *intensification* stages are plotted in Figure 7. The cyclogeostrophic balance was used to calculate the maximum value of the monthly averaged Rossby

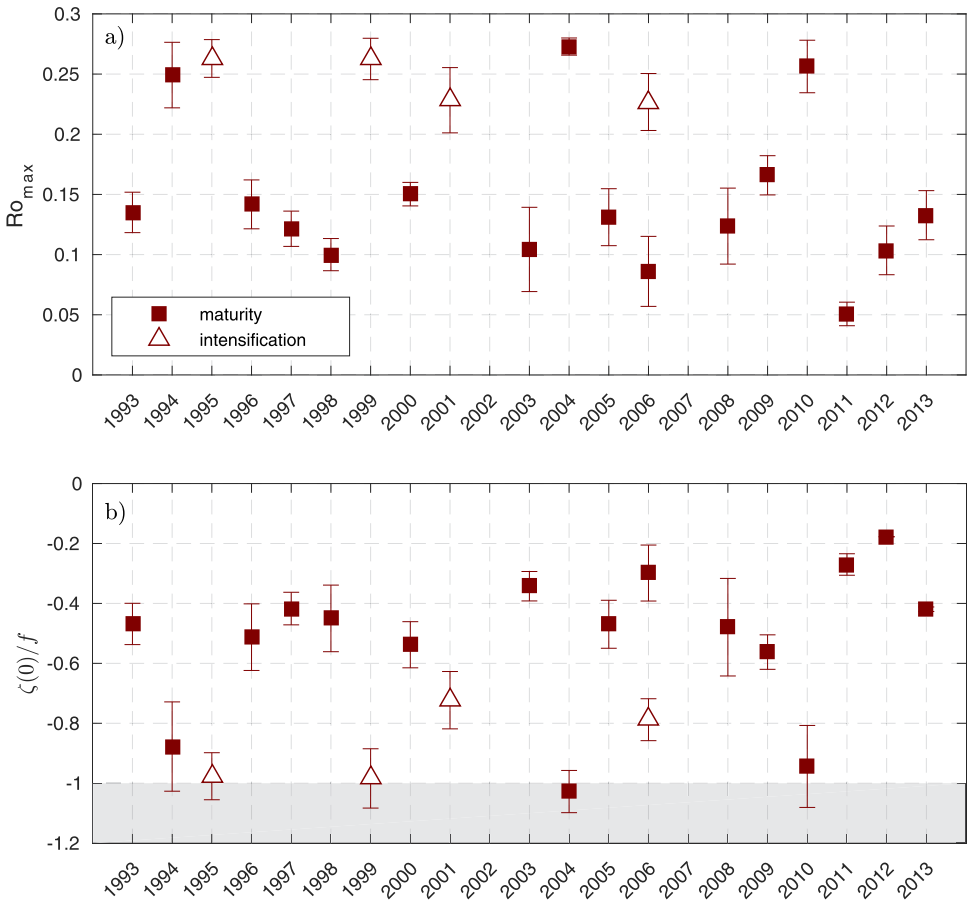

Figure 7. Extremal values of (a) the monthly mean Rossby number Ro_{max} and (b) the relative core vorticity $\zeta(0)/f=\zeta(r=0)/f$ for all the IEs detected during the 1993–2014 period. The values reached at the maturity or the intensification stages are respectively plotted with filled squares or open triangles. The errors bars correspond to the root-mean-square of the monthly fluctuations around the mean value. The gray area in the bottom figure indicates negative values of the absolute core vorticity $\zeta(0)+f < 0$.

numbers Ro_{max}. On one hand, we notice a high interannual variability of the eddies intensity especially for the *mature* stage (filled square in Figure 7) with $0.07 \leq Ro_{\max} \leq 0.27$. The maximum vortex intensity could vary by a factor 2 from 1 year to another. On the other hand, the intensity reached by the intensification of a preexisting IE is always high. Four IEs (IE94, IE98, IE00, and IE05) experience such *intensification* stage during the second year of their detection and they get similar values around $Ro_{\max}=0.23-0.27$.

We also estimate the maximum vorticity values within the eddy core. To do so, we combine the maximum Rossby number and the steepness parameter α obtained for the cyclogeostrophic velocity profile Figure 6a. Then we used equation (5) to compute the relative core vorticity $\zeta(0)/f$ reached at the *maturity* or the *intensification* stages every year Figure 6b. We confirm here that the intense vorticity value estimated by Matteoda and Glenn (1996) from the loops of a surface drifter in 1990 was not an isolated case. Quite often the core vorticity goes below $-0.5f$ in the late fall or early winter. Moreover, we found for at least 3 years (1995, 1999, and 2004), very intense values with a surface vorticity below—f in the core of the IE. Hence, such intense circular vortices are prone to inertial or symmetric instabilities (Holton, 1992; Kloosterzielt & Heijst, 1991; Mutabazi & Normand, 1992) if we neglect the effective turbulent dissipation. If it occurs, such instability could induce small-scale and three-dimensionnal perturbations at the edge of the anticyclonic structure (Kloosterzielt & Heijst, 1991; Lazar et al., 2013a; Teinturier et al., 2010).

Hence, our analysis of a long time series of altimetric measurements reveals that, during specific period of the year, the IEs are much more intense than what is generally expected for such large mesoscale eddies.

3.4.2. Spatial Variability of the IEs

According to previous studies and to Figure 1b, the climatological mean position of the IEs is centered in a specific area southeast of Crete (27°E, 34.3°N). However, such long-term temporal averaging could mask a more complex situation. We illustrate in Figure 8 the monthly mean location of the centers of all the Ierapetra anticyclones at different stages of their dynamical evolution. The first detection points, which are considered here as the formation points, are plotted in Figure 8a, top left. These formation points are not centered around the climatological mean position of IEs deduced from the 22 years averaged of the surface velocities which are computed from the mean dynamic topography (MDT). If we assume that the location of the very first formation points is driven by the strong negative wind stress curl in the summer months (Mkhinini et al., 2014) it is not surprising to find a cluster of points aligned with the mean direction of the wind shear downstream (i.e., southeast) of the Kasos strait. But, if we consider the eddy location during the maturity or the intensification stages (Figures 8b and 8c) the centers are distributed around the climatological mean position. It makes sense, because the long-term temporal averaging gives more weight to the intense eddies and therefore the climatological mean will mainly capture the spatial signature of the IEs when they reach maturity or the intensification stages. The positions of the various IEs at the end stage (i.e., the last detection point) are plotted in Figure 8, bottom. We do see here a large dispersion of the final location of the IEs with few eddies which escape from the formation area and propagate far away and reach the Libyo-Egyptian slope. Let us mention here that the automatic eddy detection and tracking algorithm as well as the SST analysis sometimes yield different IE trajectories. This rapid analysis shows that the region where the IEs gain a significant amount of kinetic energy (during the maturity or the intensification stages) is localized. It corresponds to a relatively small area centered southeast of Crete around the climatological mean position (27°E, 34.3°N).

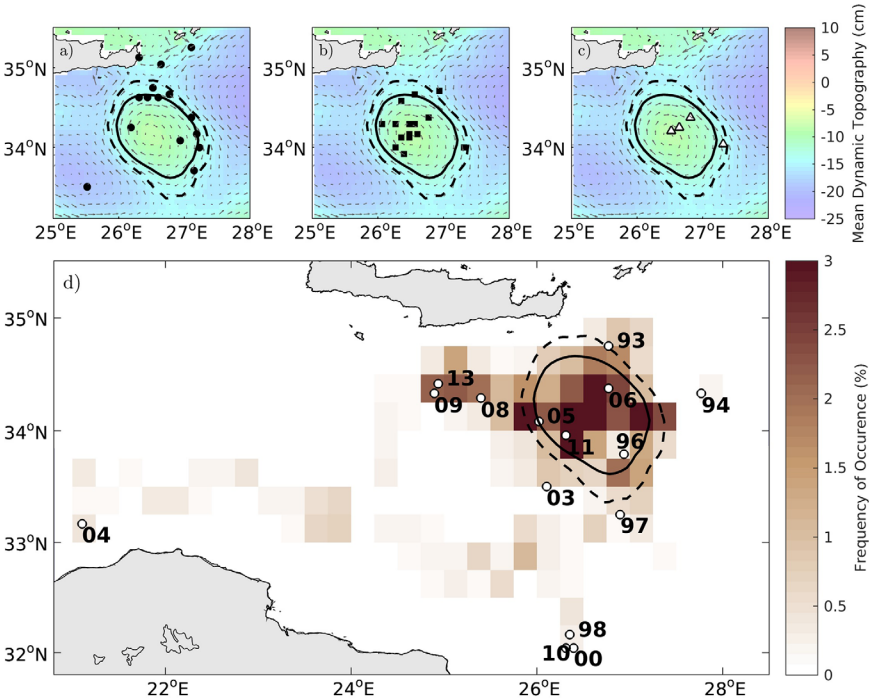

Figure 8. Monthly mean position of the centers of IEs at various stage of their dynamical evolution. The first points of detection are plotted in (a), the eddy location where they reach maturity or intensification are plotted in (b) and (c) while the point of last detection are depicted in the bottom (d). The background map and geostrophic velocity vectors correspond to the MDT while in Figure 8d, the density probability of the center position of IE is plotted. The characteristic contour and the latest contour deduced from this climatological mean are plotted in black solid and dashed lines, respectively.

4. Lifetime of the Ierapetra Anticyclone

The use of automatic eddy detection and tracking algorithm based on sea surface altimetry, which is not limited by clouds coverage or wind induced air-sea fluxes such as SST images, allows to track mesoscale eddies with no interruptions and to improve considerably the estimation of their lifetimes. Besides, we used in this study the AMEDA (Le Vu et al., 2017) which is also able to detect the merging and the splitting events (see Figure 10). Such events may indeed impact the reconstruction of the eddy trajectory and its estimated lifetime if the tracking procedure do not account for them. During the 22 years of analysis, 16 Ierapetra's were detected and their dynamical evolution is summarized in Figure 9. Each IE is labeled according to its year of formation (i.e., first detection) and the main dynamical events encountered during the eddies lifetime are indicated with specific symbols. The maturity and the intensification stages are marked respectively with black filled squares and white open triangles. The major merging events are indicated with green triangles while the few splitting events are marked with green crosses. A gray background is used when the centers of IEs remain inside the IE area (the closed contour in Figure 1b) while a white background indicates that the anticyclones escape from it and drift away.

A quick look to Figure 9 shows a large variability in the dynamical evolution of the eddies. There is no standard evolution and many distinct events could impact the eddy life time and its intensity. It is well known that IEs are long-lived eddies but we should note that most of them (9 over 15) survive at least 1 year while the longest one was tracked by the AMEDA for almost 4 years. Besides, Ierapetra anticyclones are not formed every year. When a preexisting IE is present in the formation area it will be intensified, usually in autumn, and prevent the formation of a new one. This phenomena explain why only 16 eddies were identified during the 22 years period. However, if we sum the four eddies which are intensified (IE94, IE99, IE00, and IE05) with the sixteen eddies newly formed one is missing over the 22 years period. Indeed, we did not detect any long-lasting IE formation in 2002 (the gray area in Figure 9).

During those, years several merging events between the IEs were identified and indicated with a red and dashed vertical line in Figure 9. We first recover some mergings that were mentioned in previous studies: in October 1997 the newly IE97 merges with the preexisting IE96 (Hamad et al., 2006) and at the end of June 2006 the IE05 merged with the newly formed IE06 (Mkhinini et al., 2014; Taupier-Letage, 2008). Moreover, in

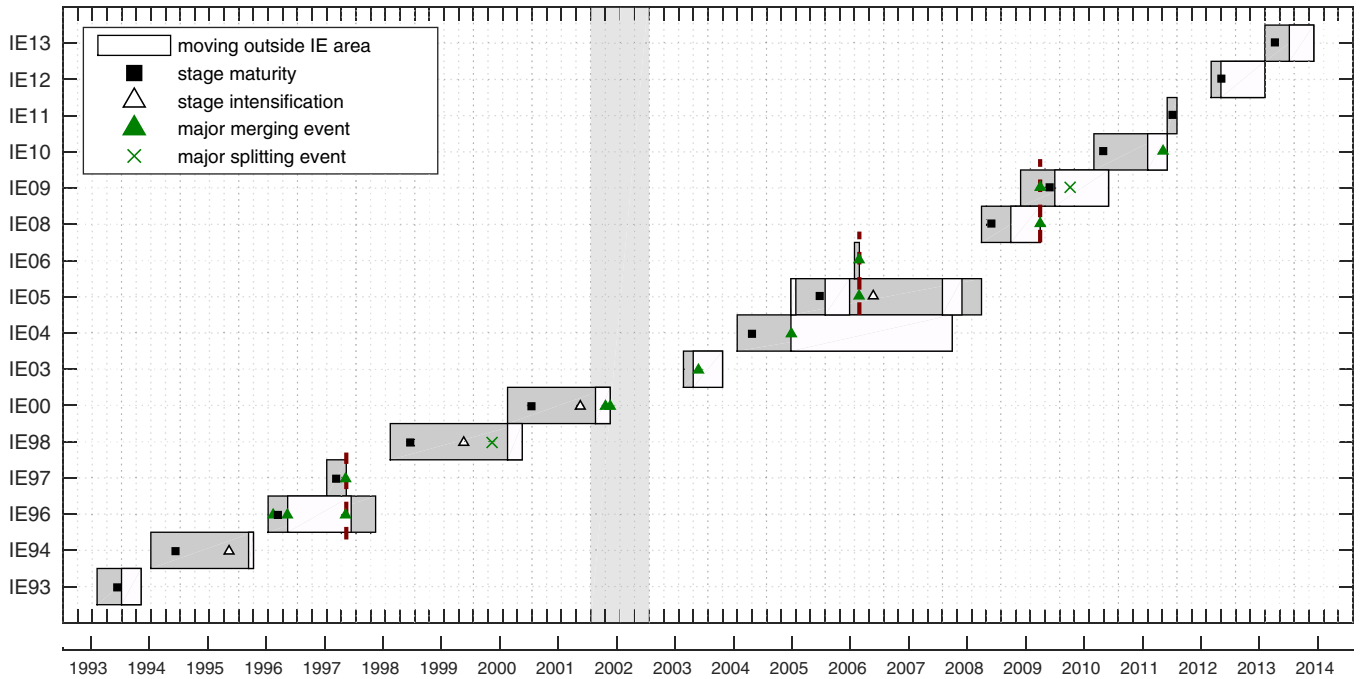

Figure 9. Chronology of the various dynamical events (formation, maturity [black square], intensification [open triangle], mergings [green triangle], or splittings [green crosses]) for all the IEs detected between 1993 and 2015. The gray (white) areas indicate the position of each IE centers inside (outside) the mean IE area depicted in Figures 1b and 8. The vertical dashed red lines indicate mergings between IEs.

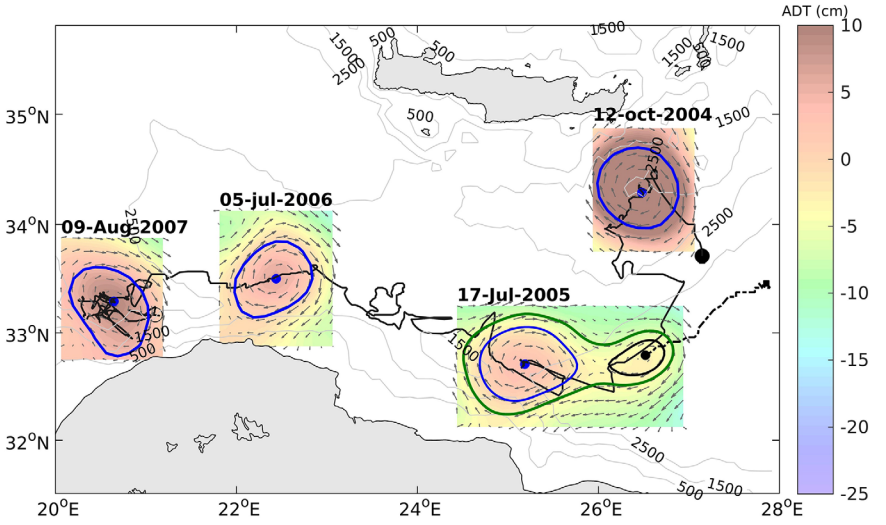

Figure 10. Full trajectory (black solid line) of the Ierapetra anticyclone IE04 from the first (23 June 2004) to the last (10 January 2008) detection point. The characteristic contour (blue line) of the anticyclone in addition to the background ADT and the velocity field are plotted at different stages of its evolution. A major merging event that occurs in July 2005 is indicated with a green contour. The trajectory (black dashed line) and the origin of the other anticyclone who merged with IE04 are also plotted.

late August 2009, the newly IE09 merges with the IE08 after 4 months of detection. However, we found at least one important merging that was not captured by the automatic tracking procedure of the AMEDA. According to SST images (see Appendix A, Figure A1) it seems that the IE05 merges in September 2008 with the newly formed IE08 while IE05 has been lost from detection by AMEDA after the 4 September 2008. This missed event is mostly due to a lack of altimetric tracks, between 29 August and 25 September, which then leads to misleading maps of gridded absolute dynamic topography for few days in this specific area. If we merge the trajectories of IE08 with IE05, the latter will then be one of the longest lived Ierapetra anticyclone that survive more than 4 years, while it could be tracked on SST images till December 2009.

On the other hand, the coexistence of IEs does not always ensure the merging between them. Sometimes, the IEs may coexist in distinct regions. We can see, for instance, in Figure 9 that the IE04 coexists for approximately 2.5 years with IE05. They remain far away from each other and their trajectories never crossed. Indeed, the oldest IE04 propagates in the south of the EMS, along the Libyo-Egyptian slope, while the IE05 remains around its formation area south of Crete Island. Another example is the newly formed IE00 which coexists with the IE98. Four months earlier the latter splits in two and the IE00 coexists with both parts for more than 3 months. This was one of the few splitting events that were detected but we should note that during the 22 years period of analysis the mergings prevail.

4.1. No IE in 2002

The fact that among the 22 years period we did not detect any formation or preexisting IEs in 2002 is puzzling. If we assume that the Etesian winds are mainly responsible for the initial formation or the intensification of Ierapetra anticyclones we should notice some specific anomaly in the seasonal wind forcing for this specific year. Following the work of Mkhinini et al. (2014), we use the same ALADIN data set (Tramblay et al., 2013) and compute the seasonal wind stress curl in summer and fall inside the *IE area* and analyse its interannual variability. We found, in comparison with the other years, a significant reduction of the summer wind stress curl by 40% in 2002. However, this correlation does not imply causation and we do believe that a full analysis on the wind-vortex interaction related to the specific formation and/or the intensification process of the IEs is the only way to understand what happens in 2002. Such dynamical analysis requires a deeper investigation which is postpone to a future paper.

4.2. IE04 Lasts 43 Months and Drifts More Than 1,200 km Away

The history of the IE04, one of the longest lived Ierapetra anticyclone that last for at least 43 months, is rare but very instructive. The location of its first detection is quite unusual. The altimetric signature of the eddy

was first detected the 23 June 2004 far away from the Kasos strait in an area where the wind stress curl is generally weak. It seems that this initial eddy, detected in June, detached from a large Libyo-Egyptian anticyclone. Unfortunately, this detachment was not identified as a splitting event by the AMEDA. Then this preexisting anticyclone enters the IE area and reaches its highest intensity at mid-October 2014 just after the strong Etesian wind forcing. The monthly mean Rossby number ($Ro \simeq 0.27$), attained at this stage, is the strongest value among all the IEs. Due to the fact, that the generation of the preexisting anticyclone does not seems to be correlated to any wind forcing and then the IE04 intensifies downward the Kasos strait, when strong wind stress curl occurs, we associate this maximum of kinetic energy to an intensification stage (rather than a maturity stage). During the 7 months that follow its intensification the IE04 slowly drifts to the southwest. Then, the AMEDA detects in May and July 2005 two successive mergings with other anticyclones. The green contour plotted in Figure 10 indicates the eddy-eddy interaction which occurs at mid-July. Hence, this large Ierapetra gain the energy of two other anticyclones who comes from the west Levantine where mesoscale anticyclones are often formed (Mkhinini et al., 2014) and where (Hamad et al., 2006; Millot & Taupier-Letage, 2005) observed that eddies accumulate and interact. These successive mergings did not affect significantly the size or the intensity of IE04 but it has probably impacted its lifetime. Indeed, this coherent structure was then tracked for more than 2 years along the Libyo-Egyptian slope until January 2008. This long and unusual trajectory of the IE04 was confirmed by a careful analysis of its SST signature. This large anticyclone that drift westward was identified as a Libyo-Egyptian eddy by previous studies (Gerin et al., 2009; Mkhinini et al., 2014; Sutyrin et al., 2009; Taupier-Letage, 2008). Several surface drifters, trapped inside the eddy from May to September 2006, and a full CTD transect, performed in May 2006 (Taupier-Letage et al., 2007, 2010), quantify the horizontal velocity and the vertical structure of this surface-intensified anticyclone (Sutyrin et al., 2009) but no connection was made with the Ierapetra eddy formed in 2004. To make such link, a complete reconstruction of the eddy trajectory that takes into account the merging with other structures should be done. It is only due to the recent improvements of the tracking procedure of the AMEDA (Le Vu et al., 2017) that such analysis becomes now possible.

We cannot ensure that the IE04 keeps the same water masses from the beginning to the end of its life. Indeed, the two mergings encountered for this specific Ierapetra anticyclone could lead to significant mixing of the water trapped in its core and therefore affect its hydrological structure. Nevertheless, according to this peculiar trajectory of the IE04, we could expect that a fraction of the initial water trapped in the southeast of Crete may travel to the south of the Levantine along the Libyo-Egyptian coast.

4.3. Relation Between the Maximum Intensity and the Lifetime

According to Figure 9, there is a high variability in the IE lifetimes ranging from 2 months to 4 years. Besides, the history of IE04 shows that many nonlinear processes, such as wind intensification or merging events could contribute to reinforce this large anticyclone and most probably extend its lifetime. In order to check if there is a correlation between the maximum amount of kinetic energy gained by an eddy and its lifetime, we plot in Figure 11 the latter as a function of the maximum Rossby number (Ro_{max}) reached by each eddy. The cyclogeostrophic balanced is taken into account to compute the Ro_{max}. We use different symbols to make the distinction between eddies who attained their maximum intensity at a maturity stage (red squares) or later on during an intensification stage (open red triangles). When the IE encounter one or several merging with other mesoscale anticyclones green triangles are used.

We first found that there is almost a linear relation between the lifetime and Ro_{max} when the eddy reached its maxima at a *maturity stage* few months after its formation. For these eddies (black squares), we can reasonably assume that they accumulate all their energy during the formation process. Then they will slowly lose their energy with time probably due to small-scale turbulent dissipation. However, few eddies deviate from this linear trend. Higher lifetimes are indeed observed when an additional amount of energy is provided by another process such as intensification (open red triangles) or merging (filled green triangles). The IE04 combines both an *intensification stage* and merging events. On the other hand, we should note that even if there is extra gain of energy the maximum eddy intensity do not exceed $Ro_{\max} < 0.28-0.3$. We suspect here that this upper bound may be due to the centrifugal-inertial instability of cyclogeostrophic anticyclones (Kloosterzielt & Heijst, 1991; Lazar et al., 2013a; Teinturier et al., 2010).

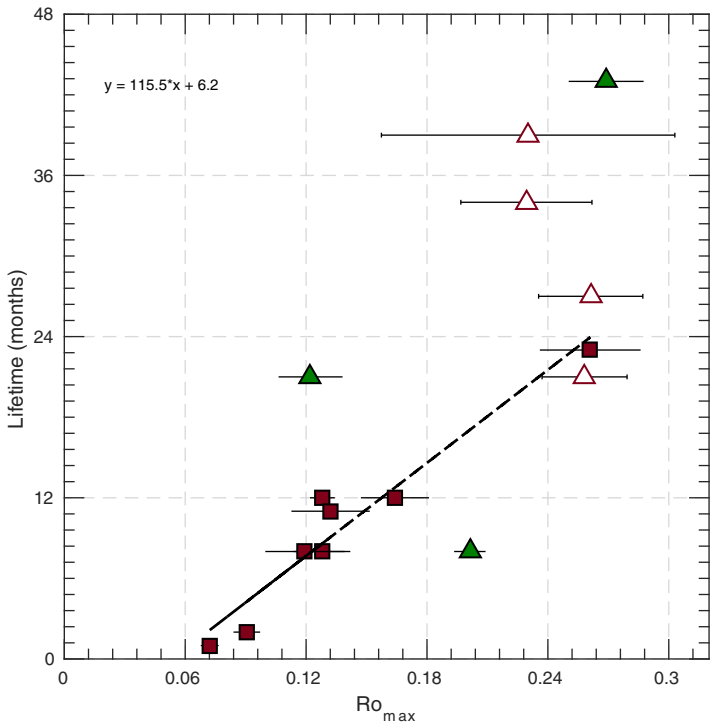

Figure 11. Lifetimes of the various IEs (tracked during the 1993–2015 period) as a function of the maximum Rossby number reached during their lifetime.

5. Comparison With In Situ Measurements

The dynamical analysis presented so far rely only on the AVISO data sets. In order to check if the altimetric products and the use of AMEDA estimate correctly the IEs intensity, we compare the previous analysis with available in situ measurements. On the contrary with the Western basin, there are very few direct measurements of the surface velocity in the Eastern Mediterranean Sea and we will mainly focus on what follows in two specific campaigns that survey the Ierapetra anticyclone: EGYPT-1 in spring 2006 and BOUM in summer 2008. Surprisingly, those two distinct oceanographic campaigns that have crossed and performed several measurements into the same eddy, the IE05 with a 2 year interval. According to AMEDA and Figure 9, the IE05 was the second most long-lived Ierapetra anticyclone, initially formed in May 2005 it survived until August 2008 for almost 4 years (up to ∼57 with SST).

5.1. EGYPT-1 Campaign

5.1.1. Drifters Measurements

Among the hundredth of SVP drifters launched during the period of the EGYPT/EGITTO program, from 2005 to 2007, few of them were launched and got trapped inside eddies (Gerin et al., 2009). Five drifters were launched in the IE05 and only two remained trapped inside the anticyclone from April to July 2006. These drifters looped inside the eddy with a typical period of 3–5 days. Hence, when filtering out these rapid oscillations on both latitude and longitude we can estimate the slow evolution of the eddy center. We calculate for each successive position $(X(t), Y(t))$ the radial distance $R(t)$ from the drifter to the eddy center. We then select specific loops corresponding to quasi-circular trajectories in the relative frame of the eddy center and we calculate, for all of them the time averaged radius R_i and the mean tangential velocity V_i. Figure 12, similar to Mkhinini et al. (2014, Figure 6a), shows the data pair (R_i, V_i) for 21 loops having a low ellipticity values: $\varepsilon < 0.3$. The intermittency of the local wind stresses or the small-scale wave activity induces dispersion in the drifter dynamics and a wide range of R_i values are then explored while the drifters loop inside the eddy. In order to compare these in situ velocity measurements with the typical velocity profile estimated from the AVISO geostrophic surface velocity, we plot in Figure 12, the mean profile $(\langle R\rangle, \langle V\rangle)$ computed by the AMEDA and averaged during the 3 months period (black solid line). We can see that all the (R_i, V_i) points are above the black curve, in other words the monthly mean velocity average of the AVISO data set underestimate the intensity of the real eddy. If we apply the cyclogeostrophic correction to this mean circular velocity profile, following the method described in section 3.3, we get closer to the in situ measurements (black dashed lines). But, it is only if we consider the most intense altimetric signal (red solid line), reached the 16 April 2006, and apply on it the cyclogeostrophic correction (dashed red line) that we were able to reach the highest azimuthal velocity values $V_{max} \simeq 35$–40 cm s^{-1} estimated from the drifter loops. Hence, if we consider only the monthly mean Rossby number obtained from the AVISO surface geostrophic velocities ($Ro \simeq 0.1$) we tend to underestimate the real eddy intensity ($Ro_{drifters} \simeq 0.132$) by 30%.

5.1.2. CTD Transect

In April 2006, a 21 CTD transect crossed the Ierapetra eddy with 18 CTD profiles, one out of two down to $1,000$ (resp. $2,000$) m depth. The typical distance between two CTD was about 8 km which is significantly less than the typical eddy radius of $R_{max} \simeq 35$–40 km. This transect was planned to cross the center of an IE according to EGYPT-1 previous CTD transects and to SST images analyzed in real time during the campaign. The superimposition of the CTD positions on the ADT map and the characteristic eddy contours computed from the surface geostrophic velocities confirms that this transect crosses the center of the IE05 at the constant latitude $\theta = 33.375°$N (Figure 13a). Then, assuming a reference level of zero velocity at $z = -1,000$ m, we can reconstruct, according to the thermal wind relation, a vertical section of the geostrophic velocity across the eddy (Figure 13b). The strong baroclinic structure of the anticyclone is clearly shown here with an intensification of the velocity within the first 100 m. However, the dynamical signature of the eddy is still

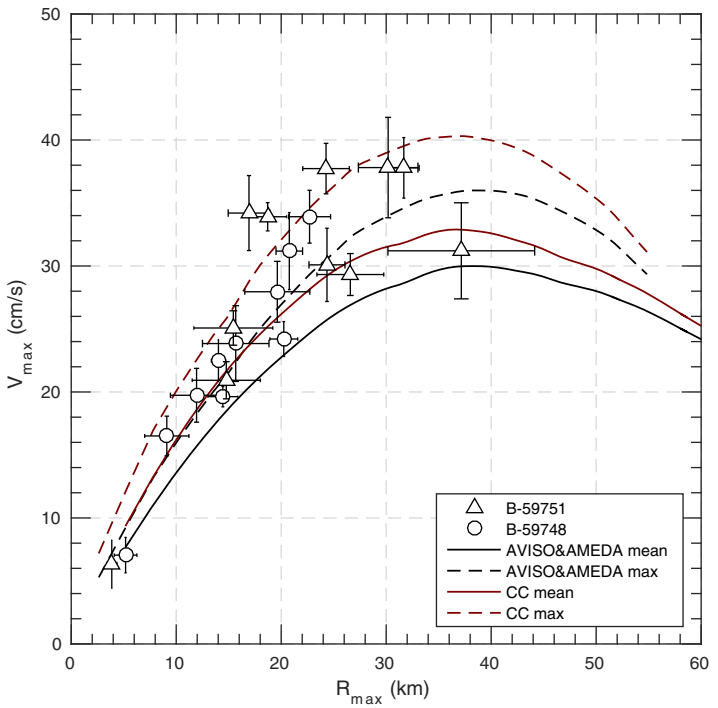

Figure 12. Points of mean tangential velocity V_i and mean eddy radius R_i with their rms error (errorbars) corresponding to the quasi-circular loops performed by the two drifters B-59751 (triangles) and B-59748 (circles) inside the IE05 from April to July 2006. The black solid line represent the 3 months mean velocity profile computed by the AMEDA applied to the AVISO data set. The red solid line depict the most intense velocity profile reached the 16 April 2006. The dashed lines indicates the cyclogeostrophic velocity profiles computed both from the mean (black) and the maximum (red) geostrophic velocity profiles.

significant at 400 m depth with typical velocity amplitudes that could reach 10–15 cm s^{-1} in the eddy core. The comparison between the surface velocity profile provided by the AVISO data set and the velocity derived from the CTD transect (averaged over the first 150 m) is shown Figure 13c. All these profiles correspond to the meridional component of the geostrophic velocity and there is no need to add any cyclogeostrophic corrections here.

We can notice that the meridional geostrophic velocities, derived from altimetric products, in the western side of the eddy, are underestimated in comparison with the in situ measurements. The geostrophic velocities derived from the CTD transect could reach 45 cm s^{-1} while the meridional velocities provided by AVISO do not exceed 32 cm s^{-1}. Hence, in the western side between (25°E–26°E) the maximal velocities derived from the *L4* altimetric products (i.e., gridded velocity fields) could be 35–40% below the measured velocities. We test the sensitivity to the vertical averaging and we did not find significant changes in the meridional velocity profile if we integrate the meridional velocities (Figure 13b) over the first 60, 100, or 150 m.

5.2. BOUM Campaign

5.2.1. CTD Measurements

Two years after the EGYPT-1 cruise the IE05 was crossed for a second time during the BOUM campaign held in 2008. After the CTD transect of April 2006 this Ierapetra anticyclone experience one major merging event: the IE05 merged with the IE06 in summer 2006, as mentioned above. Then, the IE05 passed through a strong intensification stage in autumn 2006 with a monthly mean Rossby number that reaches extremal values up to $Ro \simeq 0.22$ if the cyclogeostrophic balance is taken into account. Then the anticyclone intensity decays till spring 2007 down to $Ro = 0.06$–0.08 with a mean speed radius and maximal velocity that stayed respectively around $R_{max} = 35$–45 km and $V_{max} = 25$–30 cm s^{-1}. The IE05 was tracked by the AMEDA until early August 2008. In the last year of its detection, no major events or significant changes in size or intensity were identified. However, as it was mentioned before (section 4), according to the analysis of high-resolution SST images the IE05 seems to merge with the new IE08 formed in the late August 2008. Hence, the lifetime of Ierapetra anticyclone initially formed in 2005 probably extend to 2009 thanks to successive merging events.

The 22 and 23 June 2008, five "short duration" (SD) stations were performed in the south of Crete. The positions of the stations are plotted in comparison with the altimetric signature of the IE05 (Figure 14a). It shows that the station labeled SD6 was located inside the eddy core while the four other ones (SD4, SD5, SD7, and SD8) are outside the last closed contour (the blue dashed line in Figure 14a) of the eddy. The LADCP measurements at SD6 show surface-intensified velocities inside the IE05 in comparison with the four other stations performed outside the IE05. The estimated velocity reach quite large values, up to $V_{LADCP} = 45$–50 cm s^{-1} in the first 200 m, in comparison with the mean values ($V_{max} = 25$–30 cm s^{-1}) derived from the altimetric products. Both the velocity and the density anomaly show a strong signature of this anticyclone down to 300 m. Below, the dynamical signature is much less pronounced even if positive salinity or temperature anomalies (not shown here) could be detected down to 700 m depth.

5.2.2. VMADCP Measurements

The IE05 was crossed a second time the 30 June 2008. The VMADCP was active and thus provided direct velocity measurements through the eddy down to 200–250 m depth. The superposition of the geostrophic surface velocities with the VMADCP velocity transect Figure 15a confirms that this specific track crossed the eddy central zone (only 1 CTD). Besides, the location of two velocity maxima measured with the VMADCP are in a very good agreement with the location of the characteristic contour, the solid blue line in Figure 15a, computed by the AMEDA. More surprisingly, the vertical cross section of the meridional velocities

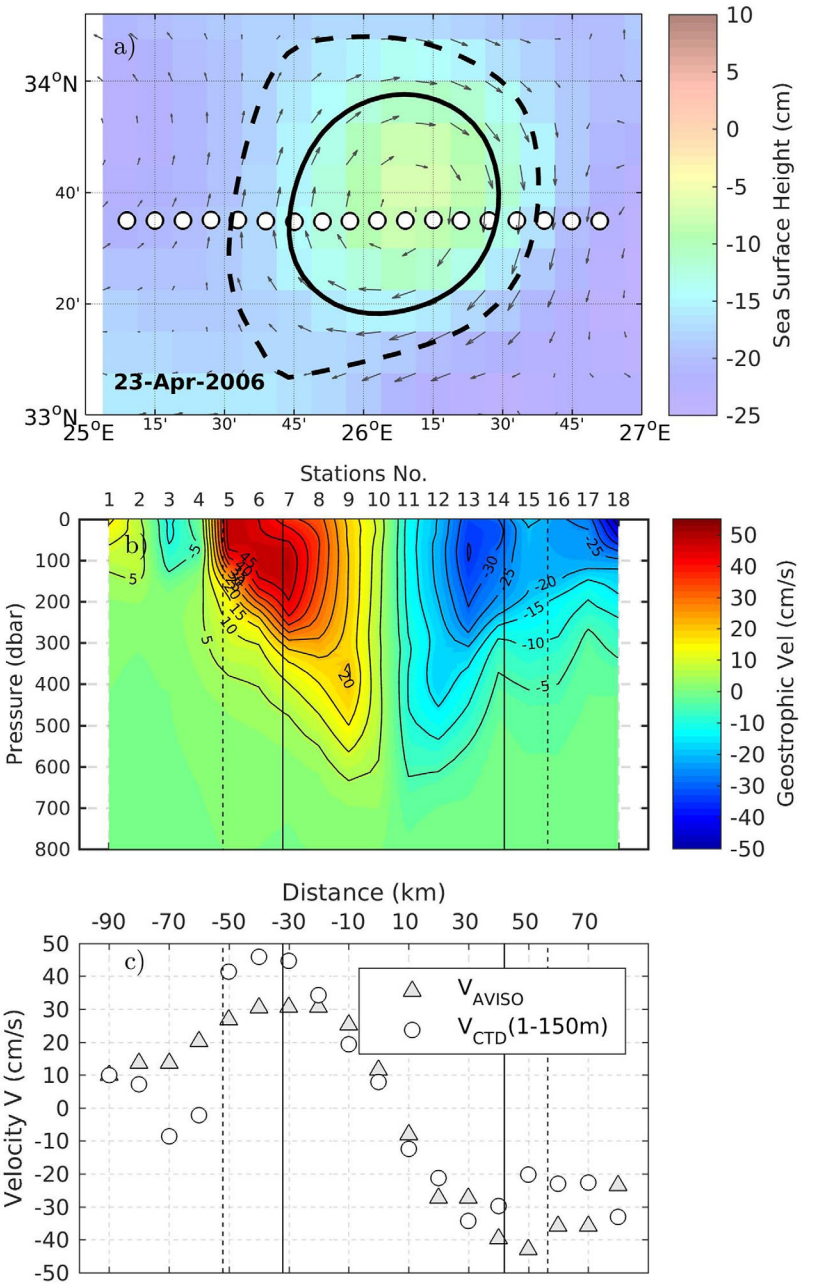

Figure 13. (a) Locations of the CTD casts performed the 23 April 2006 during the EGYPT-1/EGITTO cruise across the IE05. The meridional component of the geostrophic velocities derived from the vertical density field is plotted in (b). To apply the thermal wind relation, we used here a zero velocity level at $z=-1,000$ m. The comparison between the meridional geostrophic velocity profiles provided by AVISO or derived from the CTD transect (averaged over 150 m) is plotted in (c).

(Figure 15b) shows that the core of the IE05 is intensified below the surface. The highest velocity amplitudes, around $V_{VMADCP}=45$–$55\,\mathrm{cm\,s^{-1}}$, are reached at $z\simeq-125$ m. This subsurface intensification was not detected in the LADCP profile SD6 1 month before, even if the maximum of the velocity amplitude reach the same value. Due to the fact that the VMADCP measured the subsurface intensification on both sides of the anticyclone and at the same depth, we tend to give more confidence to the vertical structure of the velocity transect in Figure 15b rather than the LADCP profile in Figure 14b. As far as we know this is the first time that such subsurface intensification was observed for mesoscale eddies in the Eastern Basin. If the mixed layer is usually well developed in winter and often extend down to 100–150 m depth, the spring restratification may reduce the horizontal density gradient from the vortex center to its edge. Hence, due to

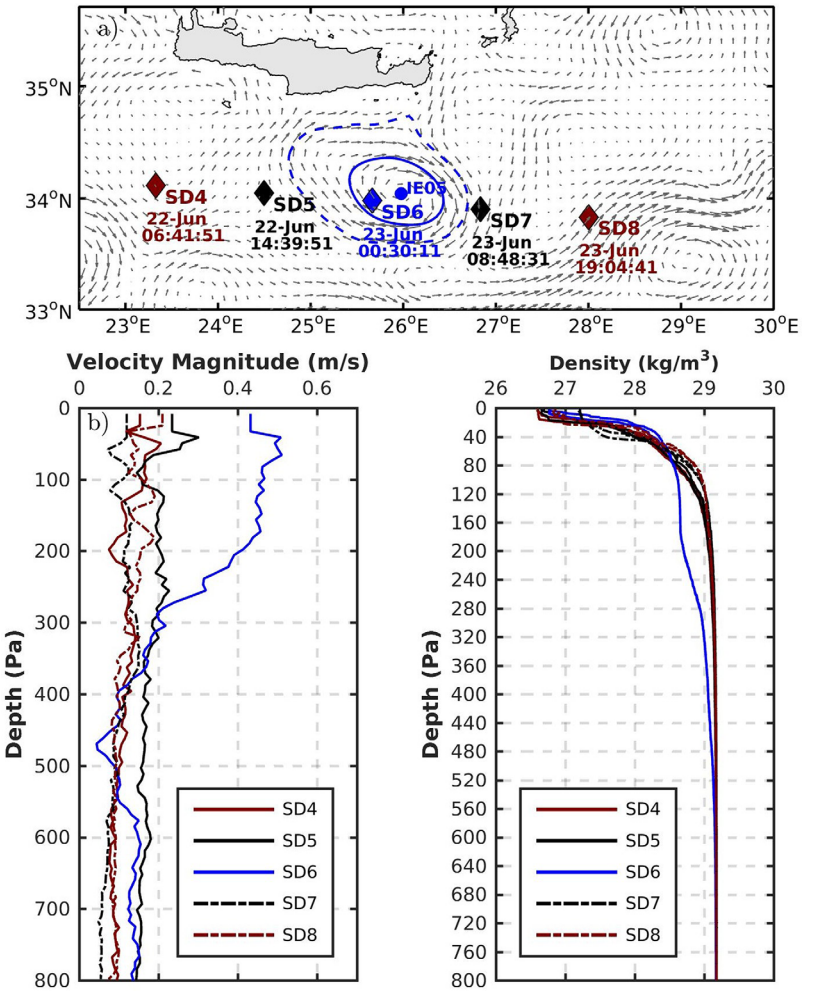

Figure 14. (a) Location of 5 CTD stations during BOUM campaign superimposed on the velocity field derived from AVISO for the 23 June 2008. The characteristic contour (solid), last contour (dashed) of the IE05 are plotted in blue. (b) The vertical velocity profile (LADCP) and (c) the density profile. The blue lines correspond to the profiles performed inside the characteristic contour of the IE05.

the geostrophic balance, the upper layer could exhibit reduced velocities in comparison with the deeper layers that were not affected by the spring restratification.

In order to perform relevant comparisons between the VMADCP measurements and the velocities, derived from altimetric measurements, it is needed to apply the cyclogeostrophic correction to the surface velocity provided by AVISO. However, due to the elliptical shape of the eddy (Figure 15a) the 30 June we cannot apply directly the equation (equation (7)) which is valid only for circular eddies. Hence, we compute with an iterative method, proposed by Penven et al. (2014) and Tuel et al. (2016), the cyclogeostrophic velocity field in a large domain around the IE center which contains the last closed streamline (i.e., the dashed blue line in Figure 15a). As we can see in Figure 15c, the cyclogeostrophic correction (red dots) is relatively weak and the meridional velocity profile is close to the geostrophic one (black dots). Both of them strongly underestimate, by at least 45%, the measured velocities (close to the surface $z=-29$ m) in the Western side of the anticyclone. The underestimation could be even stronger (60%) if we compare with the velocities measured 125 m below the surface. Hence, both in situ measurements, performed during the EGYPT-1 cruise in 2006 and the BOUM campaign in 2008, showed that if the eddy size is accurately captured by the AVISO products, the geostrophic velocities underestimate the surface velocities especially in the western side of the IE. The dynamical asymmetry between the Western and the Eastern side of the IE, in this specific area (25°E–27°E, 34°N), remain nevertheless unclear.

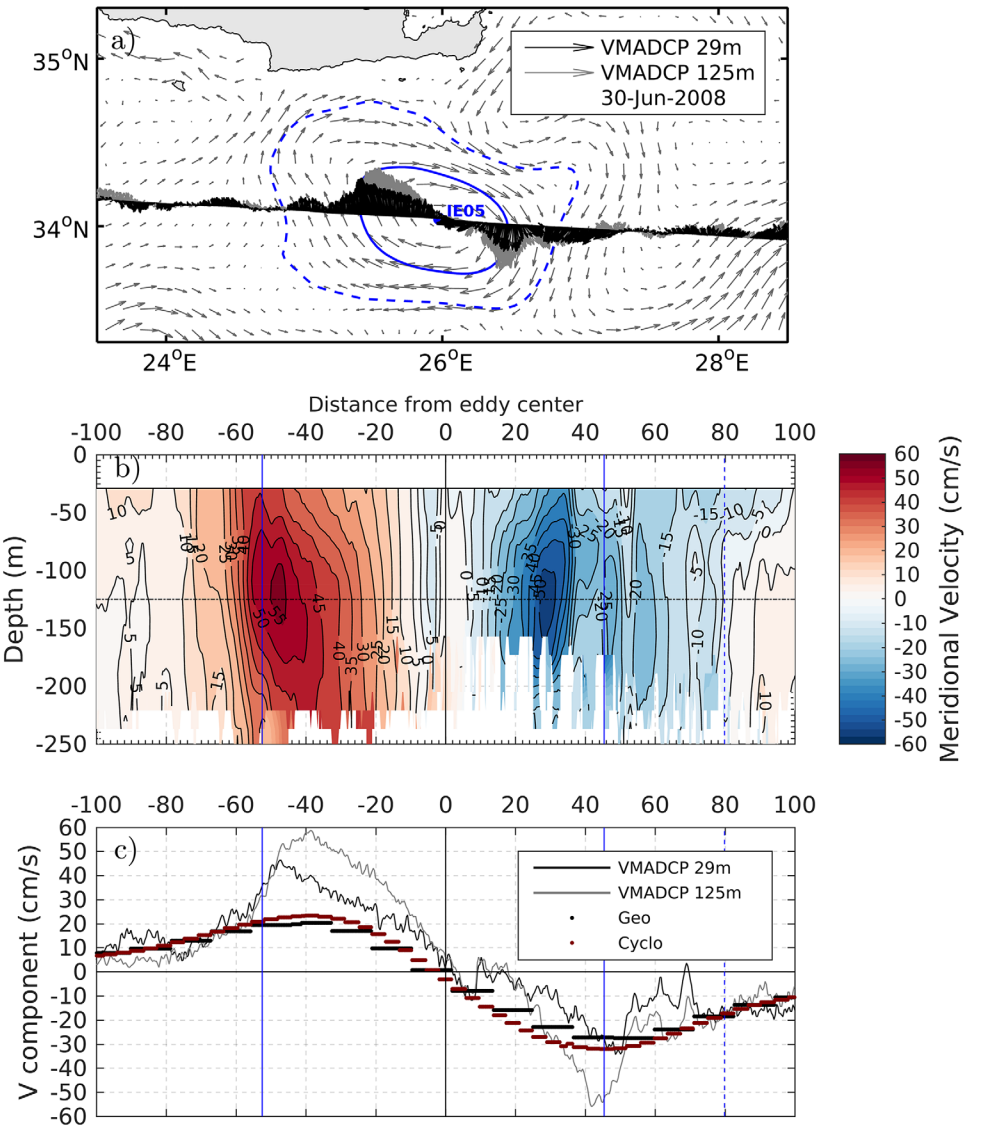

Figure 15. Vessel mounted ADCP measurements performed the 30 June 2008, when the Atalante oceanographic vessel crossed the core of IE05. The AVISO surface geostrophic velocity map is superimposed to the VMACDP transect in the top (a). The characteristic eddy contours are plotted with blue solid or dashed lines as in Figure 14a. The vertical cross section of the meridional velocity, in the first 250 m, is plotted in (b). The geostrophic (black dots) and cyclogeostrophic (red dots) velocity profiles derived from the AVISO data set are compared to the VMADCP measurements at 29 m (black line) or 125 m (gray line) in the bottom (c).

6. Conclusions

In this study, we use the *L*4 gridded products, the surface geostrophic velocities, provided by AVISO for the Mediterranean Sea and we apply the AMEDA in order to evaluate the Ierapetra eddy variability over a 22 years period from 1993 to 2014. The dynamical properties of each Ierapetra eddy (IE) were quantified and we analyzed their seasonal and interannual variabilities. Once it is formed, the eddy size remains almost constant with a mean speed radius R_{max}=30–40 km=3–4R_d. On the other hand, the IE intensity could experience significant variations with a maximal azimuthal speed V_{max} that varies from to 30 cm s^{-1} to almost 1 m s^{-1}. For such strong values, the Rossby number could exceed Ro=0.15–0.2 and the cyclogeostrophic balance should then be taken into account. The maximum eddy intensity is usually reached in fall when the IEs is located around its climatological mean position southeast of Crete (27°E, 34.3°N). The maximum

monthly mean Rossby number Ro_{max}, reached every year, experiences a strong interannual variability with Ro_{max}=0.07–0.27 and we did not detect any climatological trend over the 22 years period.

The first result was to find that the IE could be reamplified, in other words that it could gain a large amount of energy, 1 year after its formation. If previous studies were able to follow the trajectories of the long-lived Ierapetra anticyclones for several years (Hamad et al., 2006; Matteoda & Glenn, 1996; Taupier-Letage, 2008) none of them quantifies, for such a long period, the evolution of their intensity (V_{max} or Ro for instance). Following the work of Mkhinini et al. (2014) on long-lived eddies in the EMS we used a recent eddy detection and tracking algorithm able to estimate the average velocity profile (Le Vu et al., 2017) of each structure and we were therefore able to quantify the seasonal variations of the monthly mean Rossby number for each IEs. We found that the rapid increase of the vortex intensity could double the mean Rossby number in less than 4 months while keeping the mean speed radius R_{max} almost unchanged. We called such dynamical event an *intensification stage* and we make a distinction with the *maturity stage* that corresponds to the highest intensity reached just after the formation (2–4 months) of the eddy. When a preexisting IE is already present in the formation area it is likely to be intensified and therefore prevent the formation of a new one. These two distinct stages always coincide with the period of strong Etesian winds when the IEs are located in the southeast of Crete in the lee of the Kasos strait. Hence, both the formation and the intensifications of the IEs are most probably driven by the prevailing atmospheric wind stress. Nevertheless, correlation does not imply causation and the full nonlinear Ekman pumping (Dewar & Flierl, 1987; Gaube et al., 2015) should be taken into account for a correct explanation of such amplification rates. The impact of Ekman pumping and wind-eddy interactions on the *maturity* or the *intensification stages* of IEs deserve a thorough analysis and will be studied in a future work.

The second result was to find that the estimated core vorticity of the IEs could sometimes, especially during the *intensification stages*, become very strong. These large mesoscale anticyclones may even reach negative PV in their center. The previous analysis of Matteoda and Glenn (1996) and Mkhinini et al. (2014) provides some evidence of strong core vorticity but the intensity did not exceed the standard threshold $\zeta < -f$ of inertial instability (Holton, 1992; Kloosterzielt & Heijst, 1991; Mutabazi & Normand, 1992). Our analysis shows that this theoretical threshold was crossed at least three times in fall 1995, 1999, and 2004. Besides, the comparisons with in situ measurements indicate that the AVISO products tend to underestimate the maximal velocity amplitude of the IEs. Moreover, the monthly mean Rossby numbers, that we derived from the AVISO data set, also tend to smooth out extreme events. Hence, the real core vorticity is probably more intense than our estimations and the inertial instability threshold crossed more often. This type of ageostrophic instability leads to intense vertical motions at small scale and may induce a significant mixing at the vortex edge especially in the upper mixed layer where the stratification is weak (Kloosterzielt et al., 2007; Lazar et al., 2013a, 2013b). If such unstable ageostrophic perturbations do occur, the vertical mixing could be locally amplified and it will impact the heat transfer from the ocean surface to deep layers below the thermocline. The signature of the inertial instability should be found in the eddy density field with transient overturnings and layers or patches of uniform density in the periphery of the maximum velocity contour. To confirm such hypothesis, a deeper analysis of the Argo profilers or a dedicated in situ survey in the late summer or fall is needed.

Our analysis confirms that IEs are robust and coherent structures, which are predominantly located southeast of Crete in a well defined area. However, these large mesoscale eddies are not steady. We have shown that their intensity varies significantly, besides they could often merge with another anticyclone or split in two. The consecutive mergings are likely to lead to very long lifetimes that could exceed 3 years (case of IE05). The dynamical evolution and the trajectory of each individual IE is complex and does not seem to follow a general path as the Algerian Eddies in the Western Basin for instance (Escudier et al., 2016; Puillat et al., 2002). The recent development of eddy tracking algorithms (such as AMEDA) which take into account the merging and the splitting events, are needed to build these long-term trajectories and estimate the water mass transport over long distance. However, due to the spatiotemporal heterogeneity of the altimetric tracks, we are aware that the AVISO products may induce some uncertainty or errors in the eddy tracking. Therefore the complementary analysis of high-resolution satellite images (ocean color and temperature), when they are available, cannot be avoided. A reliable analysis of the trajectories of mesoscale IEs requires this double analysis. If we consider the merging of IE05 with IE08 Appendix A we can get a structure that can be tracked for more than 5 years! However, it is difficult to know the amount of mixing

in the eddy core, due to the multiple merging events, for such a complex structure. If the IEs are able to trap water masses in their core for several years, they will have a crucial impact on the distribution of heat and salt at intermediate levels, within and below the thermocline, in the EMS.

Appendix A

The figure shows the discrepancies that may occur between the automatic eddy detection and the visual inspection of SST images. We present here the evolution of the IE05 from July to September 2008, 3 years after its first detection. The contours of the eddies detected by the AMEDA applied to the AVISO data set are superimposed on the SST images. In early July 2008, Figure A1a, the location of the IE05 is in correct agreement with its signature on the SST. However, 1 month later, Figures A1b and A16c, the analysis of the AMEDA identify a merging event between IE05 and a neighboring mesoscale eddy (labeled E1) while it is clearly visible on the SST that these two anticyclones remain coherent and do not merge. At this stage the tracking procedure consider that E1 absorbed IE05 because the new eddy that results from this merging is closer in distance, size, and intensity to E1. Hence, the tracking of IE05 is stopped and if 7 days later the splitting of E1 leads to a new anticyclone E2 the later is not connected to IE05. According to the analysis of the SST images, these consecutive merging and splitting events are erroneous and the eddy labeled E2 by the AMEDA does correspond to the IE05. Then, according to the SST images (Figures A1e and A1f), the newly formed IE08 growth in early September and takes the position of E2 (i.e., the ≪ lost ≫ IE05). Hence, this final merging between the IE08 and the IE05 was not detected by the automatic analysis of the altimetric data sets. This missed event is probably due to a lack of altimetric tracks in the South of Crete between 25°E and 26°E in August 2008.

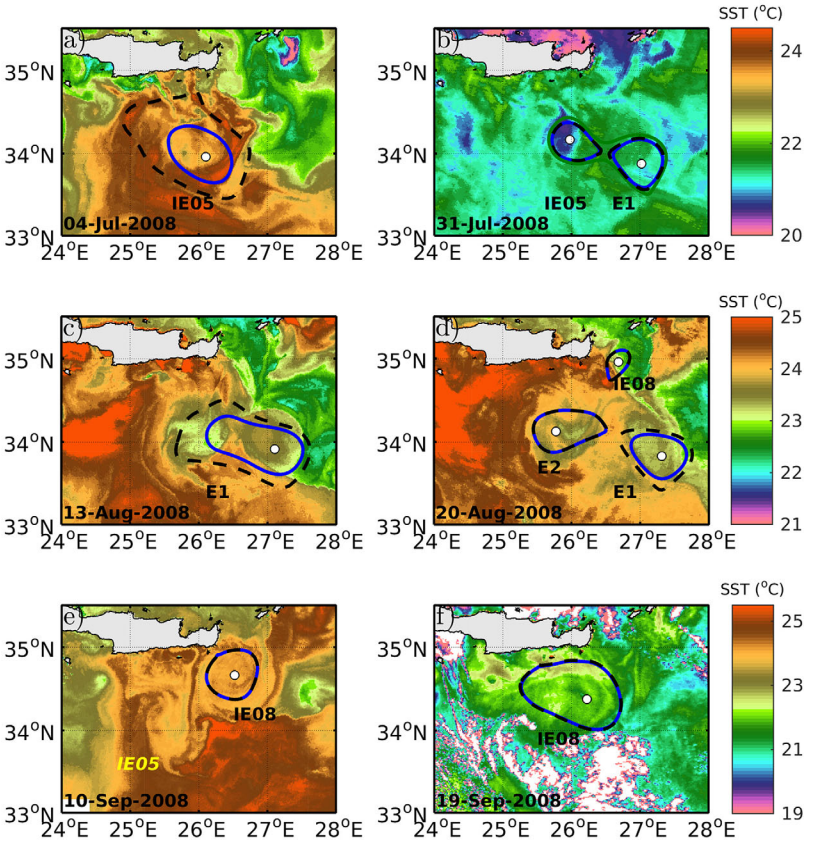

Figure A1. Images of sea surface temperature for (a) 4 July 2008, (b) 31 July 2008, (c) 13 August 2008, (d) 20 August 2008, (e) 10 September 2008, and (f) 19 September 2008. The characteristic and last eddy contours detected by AMEDA are shown with blue solid and black dashed lines. The green contour represents a merging event. The eddy names are shown with black color as tracked by AMEDA and in yellow as tracked with the SST.

Acknowledgments
This work was funded by the ANR-Astrid Project DYNED-Atlas (ANR-15-ASMA-0003-01). The authors gratefully acknowledge Thierry Moutin, Louis Prieur, and Pascale Bouruet-Aubertot for providing us the data sets of the BOUM (Biogeochemistry from the Oligotrophic to the Ultraoligotrophic Mediterranean) experiment (http://mio.pytheas.univamu.fr/BOUM/). This in situ campaign was supported by the French national LEFE-CYBER program, the European IP SESAME, and the international IMBER project. Brightness temperature images are produced by the SATMOS (CNRS INSU/MétéoFrance) at the CMS Lannion from NOAA/AVHRR images. The EGYPT program received support from INSU, LEFE-IDAO, GMMC, Euro-Argo, Région Provence-Alpes-Côte d'Azur, EGIDE-Galileo, and Coriolis. Isabelle Taupier-Letage and the MIO laboratory acknowledge the support received from the European FEDER Fund under project 1166-39417.

References

Amitai, Y., Lehahn, Y., Lazar, A., & Heifetz, E. (2010). Surface circulation of the eastern Mediterranean Levantine basin: Insights from analyzing 14 years of satellite altimetry data. *Journal of Geophysical Research*, *115*, C10058. https://doi.org/10.1029/2010JC006147

Carton, X. J., Flierl, G. R., & Polvani, L. M. (1989). The generation of tripoles from unstable axisymmetric isolated vortex structures. *Europhysics Letters*, *9*(4), 339–344. https://doi.org/10.1209/0295-5075/9/4/007

Chaigneau, A., Eldin, G., & Dewitte, B. (2009). Eddy activity in the four major upwelling systems from satellite altimetry (1992–2007). *Progress in Oceanography*, *83*(1), 117–123. https://doi.org/10.1016/j.pocean.2009.07.012

Chelton, D. B., Schlax, M. G., & Samelson, R. M. (2011). Global observations of nonlinear mesoscale eddies. *Progress in Oceanography*, *91*(2), 167–216. https://doi.org/10.1016/j.pocean.2011.01.002

Dewar, W. K., & Flierl, G. R. (1987). Some effects of the wind on rings. *Journal of Physical Oceanography*, *17*(10), 1653–1667. https://doi.org/10.1175/1520-0485(1987)017<1653:SEOTWO>2.0.CO;2

Du, Y., Yi, J., Wu, D., He, Z., Wang, D., & Fuyuan, L. (2014). Mesoscale oceanic eddies in the South China Sea from 1992 to 2012: Evolution processes and statistical analysis. *Acta Oceanologica Sinica*, *33*(11), 36–47. https://doi.org/10.1007/s13131-014-0530-6

Escudier, R., Mourre, B., Juza, M., & Tinto, J. (2016). Subsurface circulation and mesoscale variability in the Algerian subbasin from altimeter-derived eddy trajectories. *Journal of Geophysical Research: Oceans*, *121*, 6310–6322. https://doi.org/10.1002/2016JC011760

Fusco, G., Manzella, G. M. R., Cruzado, A., Gacic, M., Gasparini, G. P., Kovacevic, V., . . . Zodiatis, G. (2003). Variability of mesoscale features in the Mediterranean Sea from XBT data analysis. *Annales Geophysicae*, *21*(1), 21–32.

Gaube, P., Chelton, D. B., Samelson, R. M., Schlax, M. G., & O'Neill, L. W. (2015). Satellite observations of mesoscale eddy-induced Ekman pumping. *Journal of Physical Oceanography*, *45*(1), 104–132. https://doi.org/10.1175/JPO-D-14-0032.1

Gerin, R., Poulain, P. M., Taupier-Letage, I., Millot, C., Ismail, S. B., & Sammari, C. (2009). Surface circulation in the Eastern Mediterranean using drifters (2005–2007). *Ocean Science*, *5*(4), 559–574. https://doi.org/10.5194/os-5-559-2009

Hamad, N., Millot, C., & Taupier-Letage, I. (2005). A new hypothesis about the surface circulation in the Eastern Basin of the Mediterranean Sea. *Progress in Oceanography*, *66*(2–4), 287–298. https://doi.org/10.1016/j.pocean.2005.04.002

Hamad, N., Millot, C., & Taupier-Letage, I. (2006). The surface circulation in the Eastern Basin of the Mediterranean Sea. *Scientia Marina*, *70*(3), 457–503.

Holton, J. (1992). *An introduction to dynamic meteorology* (3rd ed., Vol. 48). San Diego, CA: Academic Press.

Horton, C., Kerling, J., Athey, G., Schmitz, J., & Clifford, M. (1994). Airborne expendable bathythermograph surveys of the eastern Mediterranean. *Journal of Geophysical Research*, *99*(C5), 9891–9905. https://doi.org/10.1029/94JC00058

Isern-Fontanet, J., Garca-Ladona, E., & Font, J. (2006). Vortices of the Mediterranean Sea: An altimetric perspective. *Journal of Physical Oceonography*, *36*(1), 87–103. https://doi.org/10.1175/JPO2826.1

JPL MUR MEaSUREs Project. (2010). *GHRSST level 4 MUR global foundation sea surface temperature analysis, version 2*. Pasadena, CA: PO.DAAC. Retrieved from https://doi.org/10.5067/GHGMR-4FJ01

Kloosterzielt, R., Carnevale, G. F., & Orlandi, P. (2007). Inertial instability in rotating and stratified fluids: Barotropic vortices. *Journal of Fluid Mechanics*, *583*, 379–412. https://doi.org/10.1017/S002211200700632

Kloosterzielt, R., & Heijst, G. V. (1991). An experimental study of unstable barotropic vortices in a rotating fluid. *Journal of Fluid Mechanics*, *223*, 1–24.

Lacombe, H., & Tchernia, P. (1972). Caractères hydrologiques et circulation des eaux en Méditeranée. In *The Mediterranean Sea: A natural sedimentation laboratory* (pp. 25–36). Stroudsburg, PA: Dowden, Hutchinson & Ross.

Larnicol, G., Ayoub, N., & Traon, P. L. (2002). Major changes in Mediterranean Sea level variability from 7 years of TOPEX/Poseidon and ERS-1/2 data. *Journal of Marine Systems*, *33–34*, 63–89. https://doi.org/10.1016/S0924-7963(02)00053-2

Larnicol, G., Traon, P.-Y. L., Ayoub, N., & Mey, P. D. (1995). Mean sea level and surface circulation variability of the Mediterranean Sea from 2 years of TOPEX/POSEIDON altimetry. *Journal of Geophysical Research*, *100*(C12), 25163–25177. https://doi.org/10.1029/95JC01961

Lazar, A., Stegner, A., Caldeira, R., Dong, C., Didelle, H., & Viboud, S. (2013a). Inertial instability of intense stratified anticyclones. Part 2. Laboratory experiments. *Journal of Fluid Mechanics*, *732*, 485–509. https://doi.org/10.1017/jfm.2013.413

Lazar, A., Stegner, A., & Heifetz, E. (2013b). Inertial instability of intense stratified anticyclones.part 1.Generalized stability criterion. *Journal of Fluid Mechanics*, *732*, 457–484. https://doi.org/10.1017/jfm.2013.412

Le Vu, B., Stegner, A., & Arsouze, T. (2017). *Angular Momentum Eddy Detection and tracking Algorithm (AMEDA) and its application to coastal eddy formation*. Retrieved from https://www.researchgate.net/publication/316360465_Angular_Momentum_Eddy_Detection_and_-tracking_Algorithm_AMEDA_and_its_application_to _coastal_eddy_formation

Li, Q.-Y., Sun, L., Liu, S.-S., Xian, T., & Yan, Y.-F. (2014). A new mononuclear eddy identification method with simple splitting strategies. *Remote Sensing Letters*, *5*(1), 65–72. https://doi.org/10.1080/2150704X.2013.872814

Malanotte-Rizzoli, P., Manca, B., d'Alcala, M. R., Theocharis, A., Bergamasco, A., Bregant, D., . . . Souvermezoglou, E. (1997). A synthesis of the Ionian sea hydrography and circulation and water mass pathways during POEM-Phase I. *Progress in Oceanography*, *39*(3), 153–204. https://doi.org/10.1016/S0079-6611(97)00013-X

Matteoda, A., & Glenn, S. (1996). Observations of recurrent mesoscale eddies in the eastern Mediterranean. *Journal of Geophysical Research*, *101*(C9), 20687–20709. https://doi.org/10.1029/96JC01111

Menna, M., Poulain, P., Zodiatis, G., & Gertman, I. (2012). On the surface circulation of the Levantine sub-basin derived from Lagrangian drifters and satellite altimetry data. *Deep Sea Research Part I: Oceanographic Research Papers*, *65*, 46–58. https://doi.org/10.1016/j.dsr.2012.02.008

Millot, C. (1985). Some features of the Algerian Current. *Journal of Geophysical Research*, *90*(C4), 7169–7176. https://doi.org/10.1029/JC090iC04p07169

Millot, C., & Taupier-Letage, I. (2005). *Circulation in the Mediterranean Sea* (pp. 29–66). Berlin, Germany: Springer. https://doi.org/10.1007/b107143

Mkhinini, N., Coimbra, A. L. S., Stegner, A., Arsouze, T., Taupier-Letage, I., & Beranger, K. (2014). Long-lived mesoscale eddies in the Eastern Mediterranean Sea: Analysis of 20 years of AVISO geostrophic velocities. *Journal of Geophysical Research: Oceans*, *119*, 8603–8626. https://doi.org/10.1002/2014JC010176

Moutin, T., & Prieur, L. (2012). Influence of anticyclonic eddies on the Biogeochemistry from the Oligotrophic to the Ultraoligotrophic Mediterranean (BOUM cruise). *Biogeosciences*, *9*, 3827–3855. https://doi.org/10.5194/bg-9-3827-2012

Mutabazi, I., & Normand, C. (1992). Gap size effects on centrifugally and rotationally driven instabillites. *Physics of Fluids A: Fluid Dynamics*, *4*(6), 1199–1205. https://doi.org/10.1063/1.858238

Nencioli, F., Dong, C., Dickey, T., Washburn, L., & McWilliams, J. (2010). A vector geometry-based eddy detection algorithm and its application to a high-resolution numerical model product and high-frequency radar surface velocities in the southern california bight. *Journal of Atmospheric and Oceanic Technology*, *27*(3), 564–579. https://doi.org/10.1175/2009JTECHO725.1

Nielsen, J. (1912). *Hydrography of the Mediterranean and adjacent waters* (pp. 77–192).
Ovchinnikov, I. (1966). Circulation in the surface and intermediate layer of the Mediterranean. *Oceanology*, *6*, 48–59.
Ovchinnikov, I., Plakhin, E., Moskalenko, L., Negliad, K., Osadchii, A., Fedoseev, A., . . . Voitova, K. (1976). *Hydrology of the Mediterranean Sea* (pp. 375). Leningrad, Soviet Union: Gidrometeoizdat.
Pascual, A., Pujol, M., Larnicol, G., Traon, P. L., & Rio, M. (2007). A mesoscale mapping capabilities of multi satellite altimetry missions:first results with real data in the Mediterranean Sea. *Journal of Marine Systems*, *65*(1–4), 190–211. https://doi.org/10.1016/j.jmarsys.2004.12.004
Penven, P., Halo, I., Pous, S., & Marié, L. (2014). Cyclogeostrophic balance in the Mozambique Channel. *Journal of Geophysical Research: Oceans*, *119*, 1054–1067. https://doi.org/10.1002/2013JC009528
Puillat, I., Taupier-Letage, I., & Millot, C. (2002). Algerian Eddies lifetime can near 3 years. *Journal of Marine Systems*, *31*(4), 245–259. https://doi.org/10.1016/S0924-7963(01)00056-2
Rio, M.-H., Poulain, P.-M., Pascual, A., Mauri, E., Larnicol, G., & Santoleri, R. (2007). A mean dynamic topography of the Mediterranean Sea computed from altimetric data, in-situ measurements and a general circulation model. *Journal of Marine Systems*, *65*, 484–508. https://doi.org/10.1016/j.jmarsys.2005.02.006
Robinson, A., & Golnaraghi, M. (1993). Circulation and dynamics of the Eastern Mediterranean Sea; quasi-synoptic data-driven simulation. *Deep Sea Research Part II: Topical Studies in Oceanography*, *40*(6), 1207–1246. https://doi.org/10.1016/0967-0645(93)90068-X
Robinson, A., Golnaraghi, M., Leslie, W. G., Artegiani, A., Hecht, A., Lazzoni, E., . . . Unluata, U. (1991). The eastern Mediterranean general circulation: Features, structure and variability. *Dynamics of the Atmosphere and the Oceans*, *15*(3–5), 215–240. https://doi.org/10.1016/0377-0265(91)90021-7
Robinson, A., Hetch, A., Pinardi, N., Bishop, J., Leslie, W., Rosentroub, Z., . . . Brenner, S. (1987). Small synoptic/mesoscale eddies and energetic variability of the eastern Levantine basin. *Nature*, *327*(6118), 131–134. https://doi.org/10.1038/327131a0
Robinson, A. R., Malanotte-Rizzoli, P., Hecht, A., Michelato, A., Roether, W., Theocharis, A., . . . Osman, M. (1992). General circulation of the Eastern Mediterranean. The POEM group (Physical Oceanography the Eastern Mediterranean). *Earth Science Reviews*, *32*, 285–309.
Schroeder, K., Garcìa-Lafuente, J., Josey, S. A., Artale, V., Nardelli, B. B., Carrillo, A., . . . Zodiatis, G. (2012). Circulation of the Mediterranean Sea and its Variability. In *The climate of the Mediterranean region* (pp. 187–256). Amsterdam, the Netherlands: Elsevier. https://doi.org/10.1016/B978-0-12-416042-2.00003-3
Stegner, A., & Dritschel, D. (2000). A numerical investigation of the stability of isolated shallow water vortices. *Journal of Physical Oceanography*, *30*(10), 2562–2573. https://doi.org/10.1175/1520-0485(2000)030<2562:ANIOTS>2.0.CO;2
Sutyrin, G., Stegner, A., Taupier-Letage, I., & Teinturier, S. (2009). Amplification of a surface-intensified eddy drift along a steep shelf in the Eastern Mediterranean Sea. *Journal of Physical Oceonography*, *39*, 1729–1741. https://doi.org/10.1175/2009JPO4106.1
Taupier-Letage, I. (2008). On the use of thermal images for circulation studies: Applications to the Eastern Mediterranean Basin. In V. Barale & M. Gade (Eds.), *Remote sensing of the European seas* (pp. 153–164). Dordrecht, the Netherlands: Springer. https://doi.org/10.1007/978-1-4020-6772-3_12
Taupier-Letage, I., Barbanti, R., El Gindy, A., Emelianov, M., & Fuda, J. (2007). New elements on the surface circulation in the Eastern Basin of the Mediterranean. In *CIESM 38th congress* (pp. 38–204). Istanbul, Turkey: International Commission for the Scientific Exploration of the Mediterranean Sea.
Taupier-Letage, I., Millot, C., Fuda, J., Rougier, G., Gerin, R., Poulain, P., . . . Sammari, C. (2010). The surface circulation in the Eastern Basin of the Mediterranean and the impact of the mesoscale eddies (Vol. 39, 189 pp.). Venice, Italy: CIESM 39th Congress, May 2010, Rapp. Comm. Int. Mer Medit.
Taupier-Letage, I., Puillat, I., Millot, C., & Raimbault, P. (2003). Biological response to mesoscale eddies in the Algerian Basin. *Journal of Geophysical Research*, *108*(C8), 3245. https://doi.org/10.1029/1999JC000117
Teinturier, S., Stegner, A., Viboud, S., & Didelle, H. (2010). Small-scale instabilities of an island wake flow in a rotating shallow-water layer. *Dynamics of Atmosphere and Ocean*, *49*(1), 1–24. https://doi.org/10.1016/j.dynatmoce.2008.10.006
Theocharis, A., Georgopoulos, D., Lascaratos, A., & Nittis, K. (1993). Water masses and circulation in the central region of the Eastern Mediterranean: Eastern ionian, South Aegean and Northwest Levantine,1986–1987. *Deep Sea Research Part II: Topical Studies in Oceanography*, *40*(6), 1121–1142. https://doi.org/10.1016/0967-0645(93)90064-T
Tramblay, Y., Ruelland, D., Somot, S., Bouaicha, R., & Servat, E. (2013). High-resolution Med-CORDEX regional climate model simulations for hydrological impact studies: A first evaluation of the ALADIN-Climate model in morocco. *Journal of Hydrology and Earth Systen Sciences*, *17*, 3721–3739. https://doi.org/10.5194/hess-17-3721-2013
Tuel, A., Stegner, A., & Le Vu, B. (2016). *Cyclogeostrophic correction of the AVISO surface velocities for intense surface eddies and its application to the Mediterranean Sea*. CIESM The Mediterranean Science Commission.
Zervakis, V., Papadoniou, G., Tziavos, G., & Lascaratos, A. (2003). Seasonal variability and geostrophic circulation in the eastern mediterranean as revealed through a repeated XBT transect. *Annales Geophysicae*, *21*(1), 33–47. https://doi.org/10.5194/angeo-21-33-2003